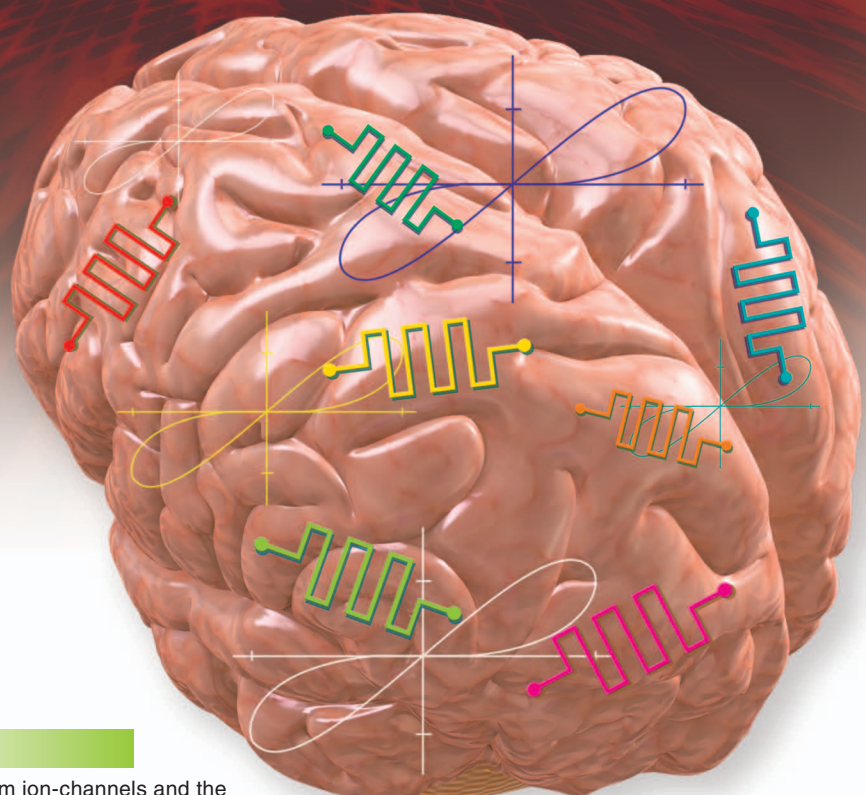


# Brains Are Made of Memristors

Maheshwar Pd. Sah,  
Hyongsuk Kim, and  
Leon O. Chua



BRAIN: IMAGE LICENSED BY INGRAM PUBLISHING & WIKIMEDIA COMMONS

## Abstract

This exposition shows that the potassium ion-channels and the sodium ion-channels that are distributed over the entire length of the axons of our neurons are in fact *locally-active memristors*. In particular, they exhibit all of the fingerprints of memristors, including the characteristic *pinched hysteresis Lissajous figures* in the voltage-current plane, whose *loop areas* shrink as the frequency of the periodic excitation signal increases. Moreover, the pinched hysteresis loops for the potassium ion-channel memristor, and the sodium ion-channel memristor, from the Hodgkin-Huxley axon circuit model are *unique* for each periodic excitation signal. An in-depth circuit-theoretic analysis and characterizations of these two classic biological memristors are presented via their small-signal memristive equivalent circuits, their frequency response, and their Nyquist plots. Just as the Hodgkin-Huxley circuit model has stood the test of time, its constituent potassium ion-channel and sodium ion-channel memristors are destined to be classic examples of locally-active memristors in future textbooks on circuit theory and bio-physics.

Digital Object Identifier 10.1109/MCAS.2013.2296414

Date of publication: 20 February 2014

## I. Introduction

The basic computation and information processing units in the brain are the *synapses* and the *axons* [1]. It is well known that *synapses are locally-passive non-volatile memristors* [2], [3]. Such memristors are essential building blocks for emulating memory and learning. But learning and other higher brain functions require that clusters of neurons be able to communicate with each other via axons depicted schematically Fig. 1(a) and Fig. 1(b). Our main goal of this exposition is to conduct an in-depth analysis of the classic *Hodgkin-Huxley circuit model* (Fig. 1(c)) of the *squid giant axons* in Fig. 1, [4] and show that it contains two *locally-active*

*memristors* which are essential for generating *action potentials (spikes)*. In particular, it contains a *potassium ion-channel memristor* and a *sodium ion-channel memristor* [5] as depicted in Fig. 1(d).

As articulated in [2] and [5] the Hodgkin-Huxley circuit model in Fig. 1(c) is conceptually wrong from a circuit-theoretic perspective because the two *time-varying* resistors are in fact *memristors*, which are *time-invariant*. In the following sections, we will present an in-depth characterization of both the potassium and the sodium ion-channel memristors. We will show that the voltage-current Lissajous figures due to a periodic input signal of both potassium and sodium memristors are *pinched hysteresis loops*, whose lobe areas shrink as the frequency of the input signal increases. These characteristics are in fact the unique *fingerprints* of memristors.

Since both the potassium and the sodium ion-channel memristors in Fig. 1(d) are the fundamental building blocks of all axons and are responsible for generating the *spikes* [6] essential for learning, adaptation, intelligence, and even consciousness, we will present a *comprehensive* in-depth characterizations of both potassium and sodium ion-channel memristors in the ensuing sections.

## II. Characterization of Pinched Hysteresis Loops

A voltage-controlled *memristor* is defined by,

$$\left. \begin{aligned} i &= G(x_1, x_2, \dots, x_n; v)v \\ \frac{dx_k}{dt} &= f_k(x_1, x_2, \dots, x_n; v), \quad k = 1, 2, \dots, n \end{aligned} \right\}, \quad (1)$$

where  $G$  in the first equation is a piecewise continuous and bounded<sup>1</sup> function of  $(x_1, x_2, \dots, x_n; v)$ , called the *memductance* of the memristor. The state variables  $(x_1, x_2, \dots, x_n)$  in the second equation depend on the internal state of the memristor and is defined by “ $n$ ” 1st-order differential equations called the associated state equations.

Similarly, a current-control memristor is defined by,

$$\left. \begin{aligned} v &= R(x_1, x_2, \dots, x_n; i)i \\ \frac{dx_k}{dt} &= f_k(x_1, x_2, \dots, x_n; i), \quad k = 1, 2, \dots, n \end{aligned} \right\}, \quad (2)$$

where  $R$  is a piecewise continuous and bounded function of  $n$  state variables  $(x_1, x_2, \dots, x_n)$ , called the *memristance* of the memristor.

One of the unique signatures of a memristor which distinguishes it from non-memristive devices is its associated *pinched hysteresis loop* in the *voltage v vs. current*

<sup>1</sup>We assume  $|G(x_1, x_2, \dots, x_n; v)| < \infty$  and  $|R(x_1, x_2, \dots, x_n; i)| < \infty$  for  $\|R(x_1, x_2, \dots, x_n)\| < \infty$ .

$i$  plane, namely, the  $v$ - $i$  loci *always* passes through *origin* for any *bipolar periodic* input voltage  $v(t)$  (resp., input current  $i(t)$ ) waveform which assumes both positive and negative voltages (resp., currents). In general, the pinched hysteresis loop may intersect itself also at additional points  $(v, i) \neq (0, 0)$ .

The shape of the pinched hysteresis loop varies with frequency  $f$  and shrinks to a single-valued function through the origin, as the frequency tends to infinity. This is another signature of a memristor. In case when the memductance  $G$  (resp., memristance  $R$ ) does not depend on  $v$  (resp.,  $i$ ), the limiting single-valued function is a straight line (Property 6 defined in [7]).

Another fingerprint of a memristor is the dependency of the hysteresis *lobe area* on the frequency  $f$  of the periodic input signal. Beyond certain critical frequency  $f^*$ , the area of the pinched hysteresis lobe *decreases monotonically* as the frequency of the periodic input voltage  $v(t)$  (resp., current  $i(t)$ ) increases.

In this section, we illustrate all these pinched hysteresis characteristics and fingerprints of the *potassium ion-channel memristor*, and the *sodium ion-channel memristor* in the classic Hodgkin-Huxley circuit model of the giant squid axon [4].

### A. Examples of Pinched Hysteresis Loops of Potassium Memristor

Chua, et. al, [5] shows the time-varying potassium conductance ( $G_K$ ) and the time-varying sodium conductance ( $G_{Na}$ ) in the Hodgkin-Huxley circuit [4] are first-order potassium memristor and second-order sodium memristor, respectively. The relationship between the input voltage  $v_K$  and the current  $i_K$  in the potassium ion channel memristor is defined by the state-dependent ohm's law,

$$\left. \begin{aligned} i_K &= G_K(n)v_K \\ \frac{dn}{dt} &= \left\{ \frac{0.01[(v_K + E_K) + 10]}{e^{\frac{(v_K + E_K) + 10}{10}} - 1} \right\} (1 - n) - \left[ 0.125 e^{\frac{(v_K + E_K)}{80}} \right] n \end{aligned} \right\} \quad (3)$$

where  $G_K(n) \triangleq \bar{g}_K n^4$  is the potassium memductance function and  $n$  is the potassium gate-activation variable. In this paper, the parameters for  $E_K$  and  $\bar{g}_K$  are assumed to be 12 mV and 36 mS/cm<sup>2</sup> respectively, as chosen by Hodgkin-Huxley [4].

The characteristics of the potassium ion channel memristor are investigated by applying several bipolar periodic signals with different initial states  $n(0)$  of the potassium state variable “ $n$ ”. The initial state  $n(0)$

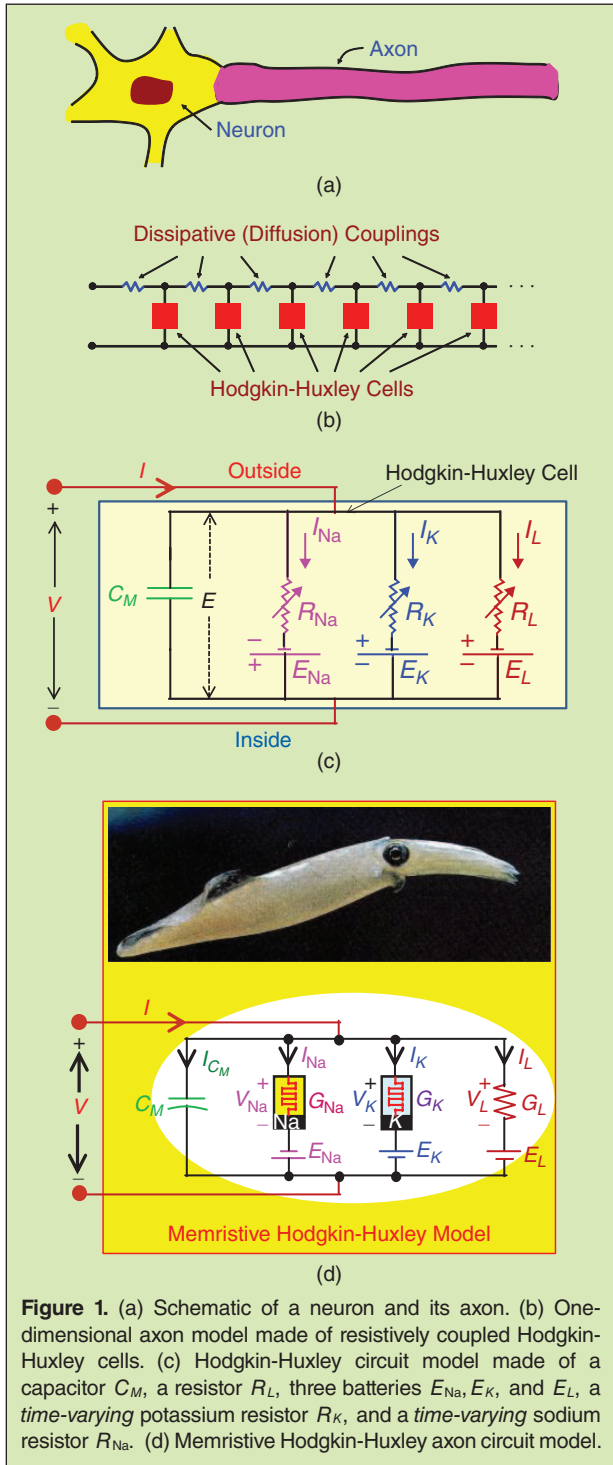


**Figure 1.** (a) Schematic of a neuron and its axon. (b) One-dimensional axon model made of resistively coupled Hodgkin-Huxley cells. (c) Hodgkin-Huxley circuit model made of a capacitor  $C_M$ , a resistor  $R_L$ , three batteries  $E_{Na}$ ,  $E_K$ , and  $E_L$ , a time-varying potassium resistor  $R_K$ , and a time-varying sodium resistor  $R_{Na}$ . (d) Memristive Hodgkin-Huxley axon circuit model.

is chosen such that the above 1st-order nonlinear differential equation, which is driven by a periodic voltage  $v_K(t)$  of period  $T = 1/f$  has a periodic response  $n(t) = n(t+T)$  for  $t \geq 0$ .

Let us apply first a sinusoidal voltage  $v_K(t) = A \sin(2\pi ft)$  with amplitude  $A = 50$  mV, and frequency  $f = 200$  Hz to the potassium ion channel memristor. Fig. 2(a) shows the waveform of the input voltage

$v_K(t)$ , output current  $i_K(t)$ , gate-activating state variable  $n(t)$ , and memductance  $G_K(t)$  respectively. The loci (Lissajous figure) of  $(v_K(t), i_K(t))$  corresponding to the input voltage  $v_K(t)$ , and current  $i_K(t)$  is shown in Fig. 2(b). Note that it passes through the origin at point ① and ③, respectively. Moreover, observe that the memductance  $G_K(t)$  in Fig. 2(a) is always positive. The upper figure in Fig. 2(b) is a double-valued Lissajous figure plotted in  $i_K$  vs.  $v_K$  plane. Such a multi-valued Lissajous figure of  $v(t)$  and  $i(t)$  which *passes through the origin* is called a *pinched hysteresis loops* in footnote 12, page 1850 of [8]. The lower figure in Fig. 2(b) shows the variation of the potassium memductance  $G_K$  of the potassium ion-channel memristor with respect to the applied voltage  $v_K(t)$ .

Consider next a potassium ion-channel memristor driven by a composite waveform consisting of a sinusoidal voltage  $A \sin(2\pi ft)$  and its  $N$ th harmonic of amplitude  $B$  and phase angle  $\theta$ ; namely  $v_K(t) = A \sin(2\pi ft) + B \sin(2\pi Nft + \theta)$ , where “ $N$ ” denotes the order of the harmonics of the sinusoidal signal  $A \sin(2\pi ft)$  from Fig. 2(a). Fig. 3(a) shows the pinched hysteresis loop corresponding to the frequency  $f = 100$  Hz,  $A = B = 40$ ,  $\theta = \pi/3$  and  $N = 1, 3, 5, 8$ . As the value of  $N$  is varied, the input signal is modulated, resulting in a “multi-lobe” pinched hysteresis loci in the  $i_K$  vs.  $v_K$  plane. A family of pinched loops with multiple lobes obtained for  $N = 1, 3, 5$ , and 8, are shown in Fig. 3(b). Observe from Fig. 3(a) and Fig. 3(b) that even though there are multiple lobes in the  $i_K$  vs.  $v_K$  plane, all loops are pinched at the origin.

Consider a potassium ion channel memristor driven by several distinct bipolar input signals, namely  $v_K(t) = A \sin(2\pi ft)$ ,  $v_K(t) = A \cos(2\pi ft)$ ,  $v_K(t) = A \sin(2\pi ft) + B \cos(2\pi ft)$  and  $v_K(t) =$  a rectangular waveform. As expected, the loci in the  $i_K$ - $v_K$  plane for these input signals exhibit pinched hysteresis loops at the origin as shown in Fig. 4. Observe also, the shape of the pinched hysteresis loops shrinks as the frequency of the input signal increases. All these pinched hysteresis loops exhibit the fingerprints of a memristor.

### B. Examples of Pinched Hysteresis Loops of Sodium Ion-Channel Memristor

The governing equations of the sodium ion channel memristor is defined by,

$$\begin{aligned} i_{Na} &= G_{Na}(m, h) v_{Na} \\ \frac{dm}{dt} &= \left\{ \frac{0.1[(v_{Na} - E_{Na}) + 25]}{e^{\frac{(v_{Na} - E_{Na}) + 25}{10}} - 1} \right\} (1 - m) - \left[ 4e^{\frac{v_{Na} - E_{Na}}{18}} \right] m \\ \frac{dh}{dt} &= \left\{ 0.07e^{\frac{(v_{Na} - E_{Na})}{20}} \right\} (1 - h) - \left[ \frac{1}{e^{\frac{(v_{Na} - E_{Na}) + 30}{10}} + 1} \right] h \end{aligned} \quad (4)$$

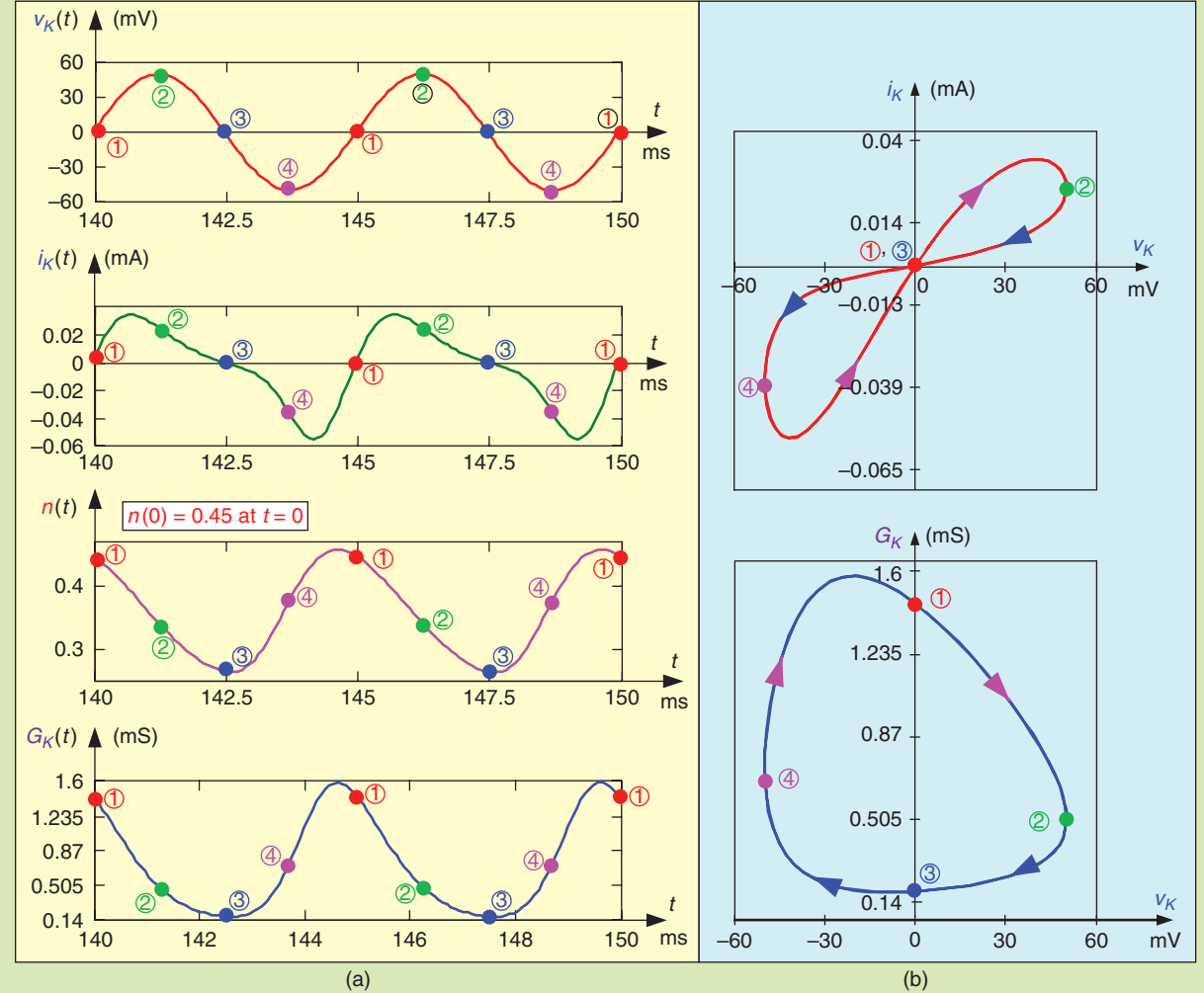


**Figure 2.** (a) Waveforms of the applied voltage  $v_K(t) = A \sin(2\pi ft)$ , current  $i_K(t)$ , state variable  $n(t)$ , and memductance  $G_K(t)$  of the potassium ion-channel memristor. (b) Potassium pinched hysteresis loop in  $i_K$  vs.  $v_K$  plane and corresponding variation of the potassium memductance  $G_K$  with respect to the applied sinusoidal voltage. The simulations were performed at  $A = 50$  mV,  $f = 200$  Hz and  $n(0) = 0.45$ .

where  $G_{\text{Na}}(m, h) \triangleq \bar{g}_{\text{Na}} m^3 h$  is the sodium memductance function, “ $m$ ” is the sodium gate-activation state variable, and “ $h$ ” is the sodium gate inactivation state variable. In this paper, the parameters for  $E_{\text{Na}}$  and  $\bar{g}_{\text{Na}}$  are equal to 115 mV and 120 mS/cm<sup>2</sup> respectively, as chosen by Hodgkin and Huxley [4].

Let us illustrate the characteristic features of the sodium ion channel memristor by applying various bipolar signals with appropriate initial states  $m(0)$  and  $h(0)$  such that the solution of the two nonlinear differential equations in (4) when driven by a periodic signal has a periodic response, for  $t \geq 0$ .

Fig. 5(a) shows the waveforms of the applied input voltage  $v_{\text{Na}}(t) = A \sin(2\pi ft)$ , current  $i_{\text{Na}}(t)$ ,  $m(t)$ ,  $h(t)$  and the sodium memductance  $G_{\text{Na}}(t)$  of the sodium ion-channel memristor, respectively. The corresponding

Lissajous figure of  $i_{\text{Na}}$  vs.  $v_{\text{Na}}$ , and  $G_{\text{Na}}$  vs.  $v_{\text{Na}}$  are shown in Fig. 5(b). Observe that they are “Pinched” not only at the origin, but also at point ②=point ⑤. The self-crossing of the  $v_{\text{Na}}-i_{\text{Na}}$  pinched hysteresis loop and the memductance  $G_{\text{Na}}$  hysteretic loop corresponding to point ② (resp., point ⑤) are numerically found to be  $i_{\text{Na}} = 0.022$  mA,  $v_{\text{Na}} = 69.31$  mV, and  $G_{\text{Na}} = 0.319$  mS, respectively.

When a sodium ion-channel memristor is driven by a composite waveform such as  $v_{\text{Na}}(t) = A \sin(2\pi ft) + B \sin(2\pi Nft + \theta)$ , where “ $N$ ” denotes the order of the harmonics of  $A \sin(2\pi ft)$  the characteristic of the pinched loop changes with  $A, B, \theta$  and  $N$ . Fig. 6(a) shows the pinched hysteresis loop corresponding to the frequency  $f = 500$  Hz,  $A = B = 50$  mV,  $\theta = \pi/3$  and  $N = 1, 3, 5, 8$  and Fig. 6(b) shows the corresponding pinched hysteresis

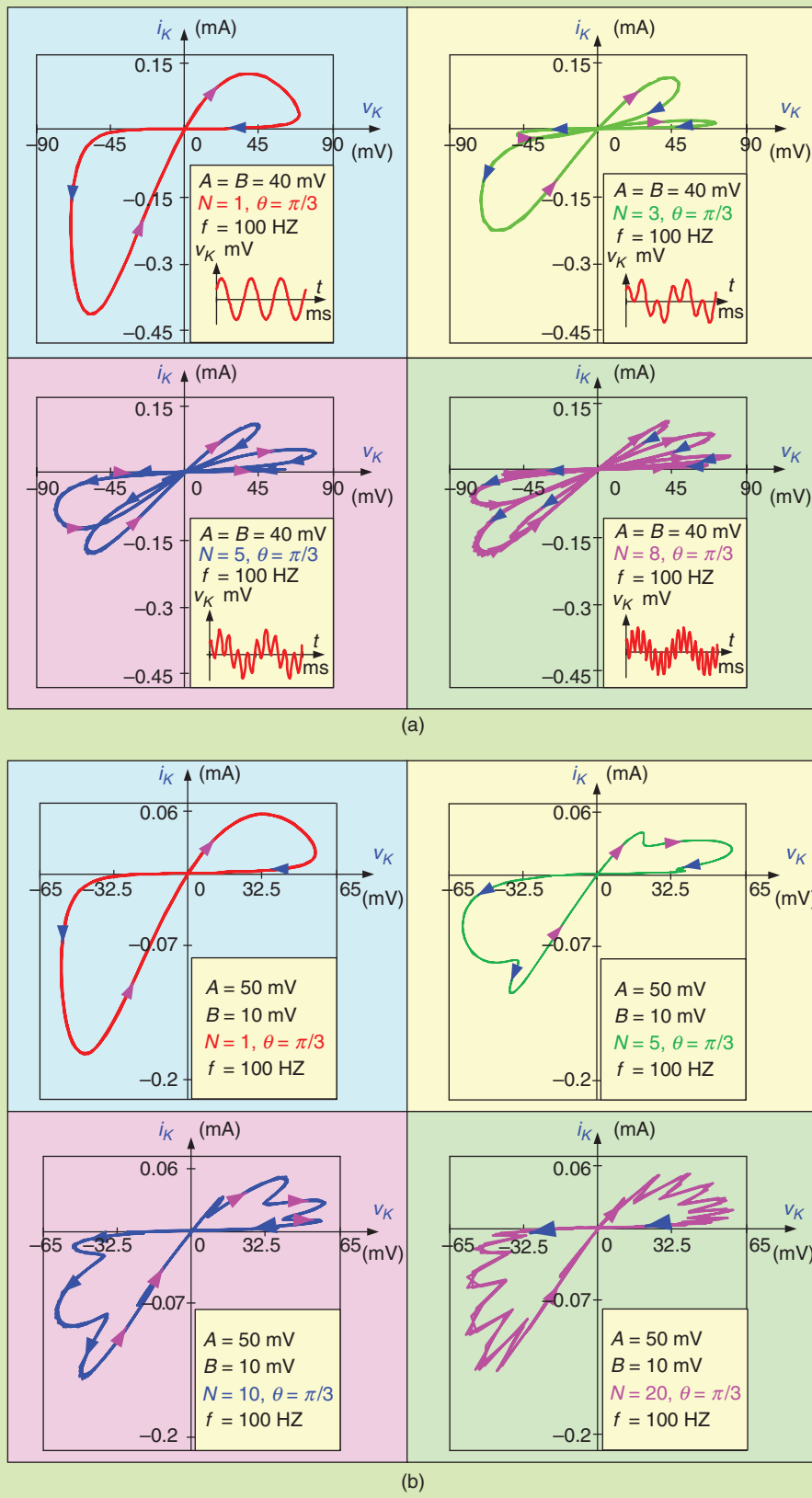


**Figure 3.** Pinched hysteresis loops of the potassium ion channel memristor for input voltage  $v_K(t) = A \sin(2\pi ft) + B \sin(2\pi Nft + \theta)$ , with  $f = 100 \text{ Hz}$  and  $\theta = \pi/3$ . (a) Pinched hysteresis loops for  $A = B = 40 \text{ mV}$ , and  $N = 1, 3, 5, 8$ . (b) Pinched hysteresis loops for  $A = 50 \text{ mV}, B = 10 \text{ mV}$  and  $N = 1, 5, 10, 20$ .

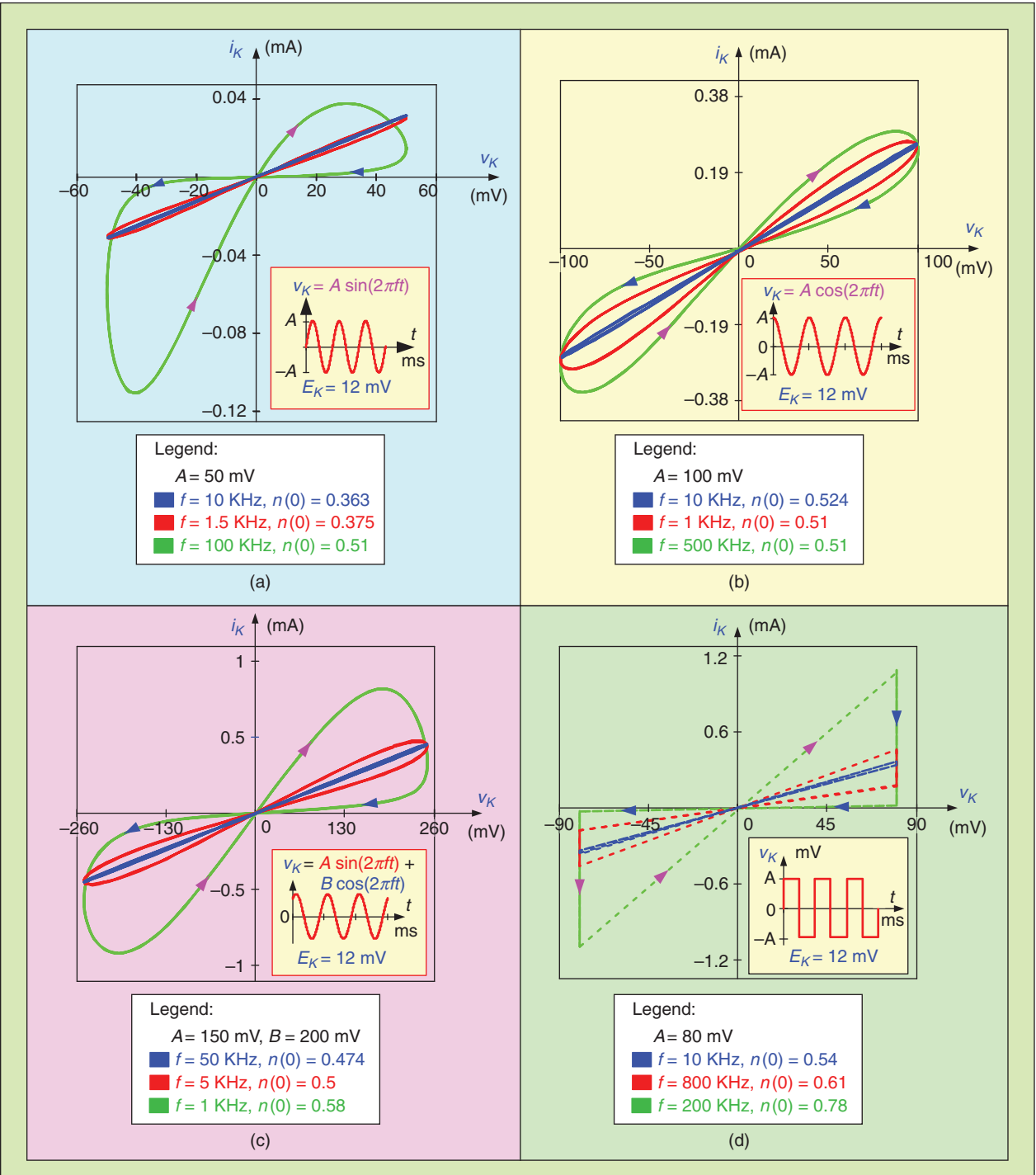
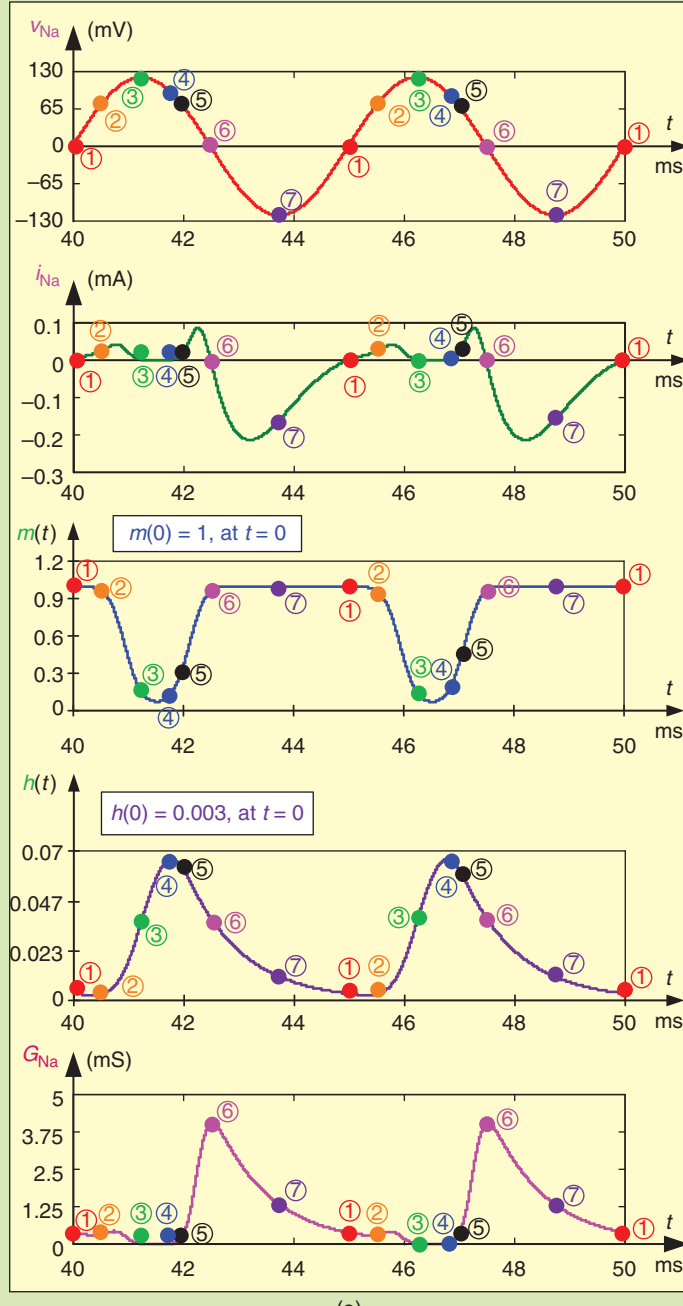


**Figure 4.** Pinched hysteresis loops of the potassium ion channel memristor for various bipolar periodic input signals. (a)  $v_K(t) = A \sin(2\pi ft)$ . (b)  $v_K(t) = A \cos(2\pi ft)$ . (c)  $v_K(t) = A \sin(2\pi ft) + B \cos(2\pi ft)$ . (d) A rectangular waveform. The dotted lines in Fig. 4(d) indicate instantaneous jump of  $v_K$  and  $i_K$  at  $t = 0, T/2, \text{ and } T$ .

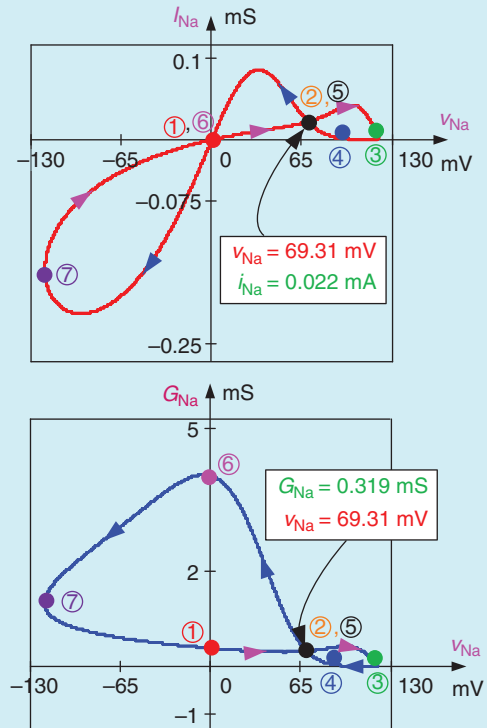
loops for  $f = 500$  Hz,  $A = 50$  mV,  $B = 15$  mV,  $\theta = \pi/3$ , and  $N = 1, 5, 10$  and  $20$ .

Fig. 7 shows the pinched hysteresis loops of the sodium ion-channel memristor for  $v_{Na}(t) = A \sin(2\pi ft)$ ,  $v_{Na}(t) = A \cos(2\pi ft)$ ,  $v_{Na}(t) = A \sin(2\pi ft) + B \cos(2\pi ft)$

and  $v_{Na}(t) =$  a rectangular waveform for several different frequencies. Observe that the area of the pinched hysteresis loops shrinks with the frequency  $f$  and tend to a straight line as predicted. All these pinched hysteresis loops exhibit the fingerprints of the memristor.



(a)



(b)

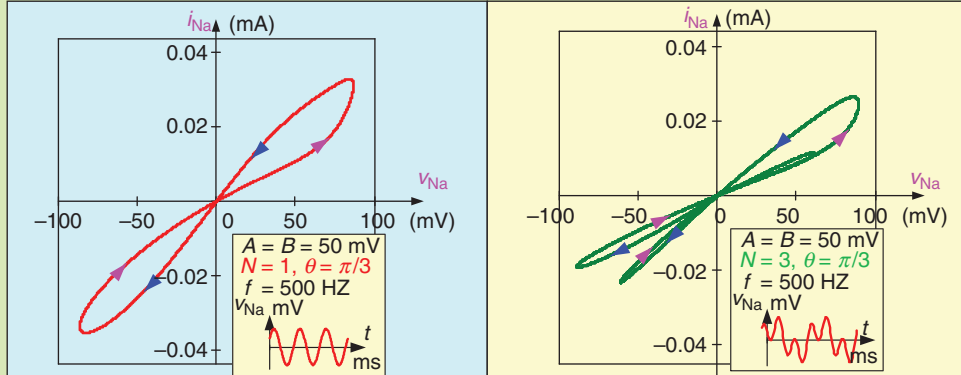
**Figure 5.** An example of a memristor exhibiting self-crossing pinched hysteresis loop in  $i_{Na}$  vs.  $v_{Na}$  and  $G_{Na}$  vs.  $v_{Na}$  plane at  $v_{Na}(t) \neq 0$  (resp. current  $i_{Na}(t) \neq 0$ ). (a) Waveforms of the input voltage  $v_{Na}(t) = A \sin(2\pi ft)$ , current  $i_{Na}(t)$ ,  $m(t)$ ,  $h(t)$ , and the sodium memductance  $G_{Na}(t)$  of the sodium ion-channel memristor. (b) Corresponding  $v_{Na}$ - $i_{Na}$  pinched hysteresis loop and the sodium memductance  $G_{Na}$  hysteretic loop plotted in  $i_{Na}$  vs.  $v_{Na}$  plane and the  $G_{Na}$  vs.  $v_{Na}$  plane, respectively. The simulations were performed at  $A = 120$  mV,  $f = 200$  Hz,  $m(0) = 1$ , and  $h(0) = 0.003$ .

### C. Computation of Lobe Area of Pinched Hysteresis Loop Via Riemann–Stieltjes Integral

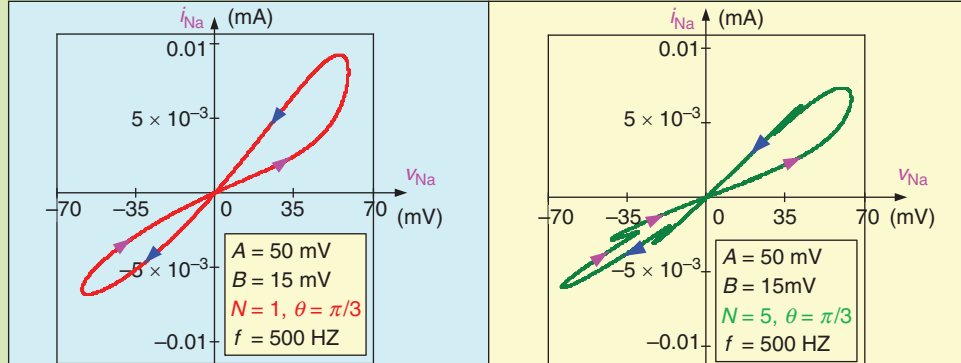
When a memristor is driven by a bipolar periodic input voltage  $v(t)$  or current  $i(t)$ , the pinched hysteresis loop has a typical shape depending on the memristor

constitutive relation. Above a certain critical frequency  $f_c$ , the area of the hysteresis lobe in the 1st or 3rd quadrant<sup>2</sup> is inversely proportional to the excitation

<sup>2</sup>Assuming each lobe is enclosed by a simple closed curve without self-intersections except at the origin.



(a)



(b)

**Figure 6.** Pinched hysteresis loops of the sodium ion channel memristor for input voltage  $v_{\text{Na}}(t) = A \sin(2\pi ft) + B \sin(2\pi Nft + \theta)$ , with  $f = 500 \text{ Hz}$ ,  $\theta = \pi/3$ . (a) Pinched hysteresis loops for  $A = B = 50 \text{ mV}$ , and  $N = 1, 3, 5, 8$ . (b) Pinched hysteresis loops for  $A = 50 \text{ mV}$ ,  $B = 15 \text{ mV}$  and  $N = 1, 5, 10, 20$ .

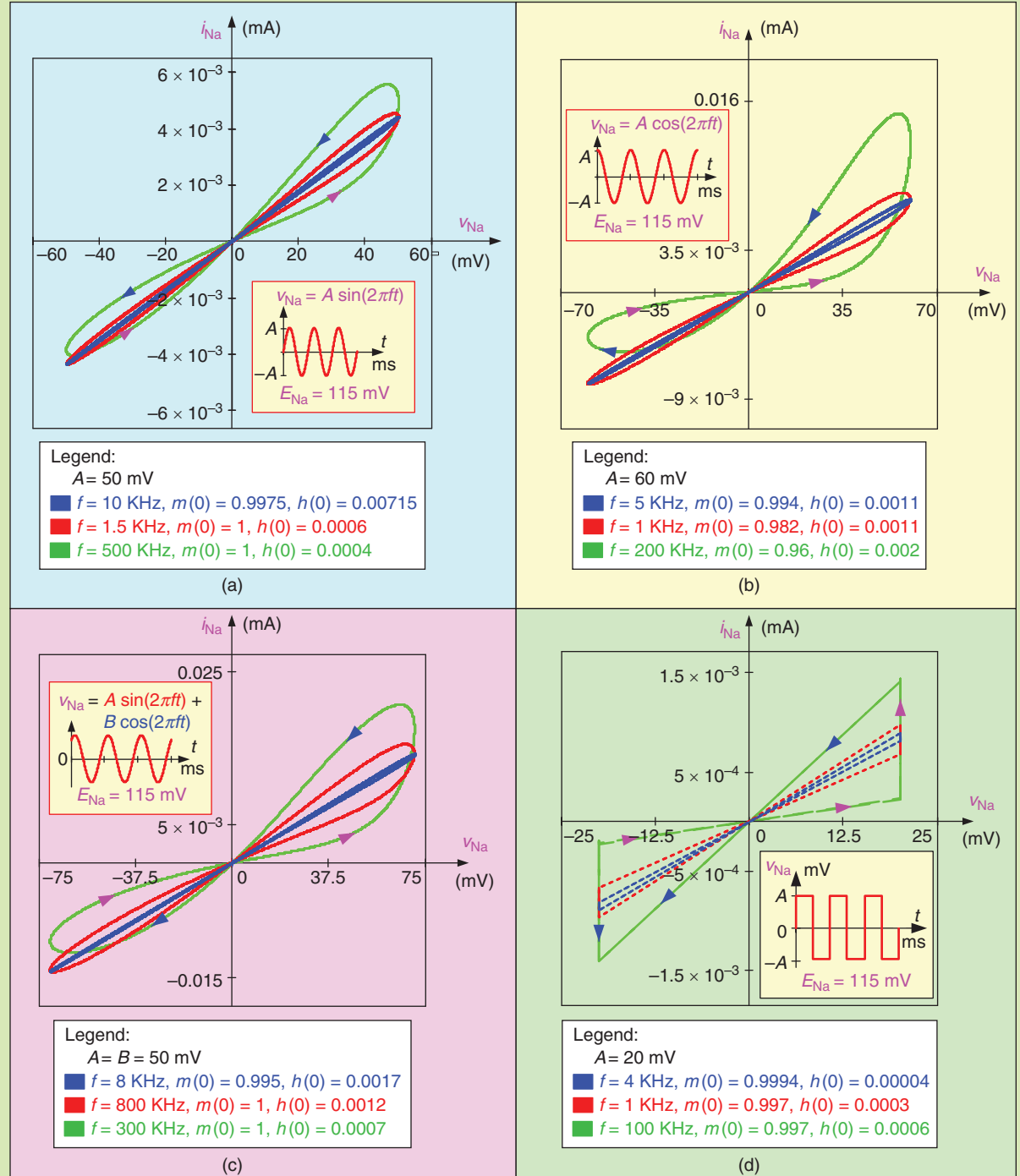


**Figure 7.** Pinched hysteresis loops of the sodium ion-channel memristor for different bipolar periodic input signals. (a)  $V_{\text{Na}}(t) = A \sin(2\pi ft)$ . (b)  $V_{\text{Na}}(t) = A \cos(2\pi ft)$ . (c)  $V_{\text{Na}}(t) = A \sin(2\pi ft) + B \cos(2\pi ft)$ . (d)  $V_{\text{Na}}(t) = a \text{ rectangular waveform}$ . The dotted lines in Fig. 7(d) correspond to an instantaneous jump at  $t = 0, T/2$ , and  $T$ .

frequency  $f$ . Thus, the area of the pinched lobe gradually decreases with increasing frequency for  $f > f_c$ . The frequency dependence characteristic of the *lobe area* is another signature property of a memristor.

Let us apply a bipolar periodic input signal to a memristor such that a pinched hysteresis loop in the 1st and 3rd quadrants is obtained during the positive ( $0 \leq t \leq T/2$ ) and the negative ( $T/2 \leq t \leq T$ ) signal

amplitudes, respectively. To compute the area enclosed within the pinched hysteresis loop in the 1st and 3rd quadrants, respectively, let us first consider the pinched hysteresis loop only over the bounded time interval  $0 \leq t \leq T/4$  in the  $i$ - $v$  plane as shown in the Fig. 8(a). As proposed by Chua in [2], the yellow area under the curve of Fig. 8(a) can be computed via the following *Riemann–Stieltjes Integral* [9]:

$$Ar_1 = \int_0^{T/4} i(t) \frac{dv(t)}{dt} dt > 0. \quad (5)$$

Similarly, the cyan area under the curve for interval  $T/4 \leq t \leq T/2$  of Fig. 8(b) can be computed as follows:

$$Ar_2 = \int_{T/4}^{T/2} i(t) \frac{dv(t)}{dt} dt < 0. \quad (6)$$

Adding (5) and (6), we get the 1st quadrant green lobe area shown in Fig. 8(c). It follows, that the 1st quadrant lobe area ( $Ar^+$ ) of the pinched hysteresis loop for the half cycle  $0 \leq t \leq T/2$  is given by,

$$\begin{aligned} Ar^+ &= \int_0^{T/4} i(t) \frac{dv(t)}{dt} dt + \int_{T/4}^{T/2} i(t) \frac{dv(t)}{dt} dt \\ &= \int_0^{T/2} i(t) \frac{dv(t)}{dt} dt, \end{aligned} \quad (7)$$

which can be interpreted as the *Riemann–Stieltjes Integral* of  $i(t)$  with respect to  $v(t)$ .

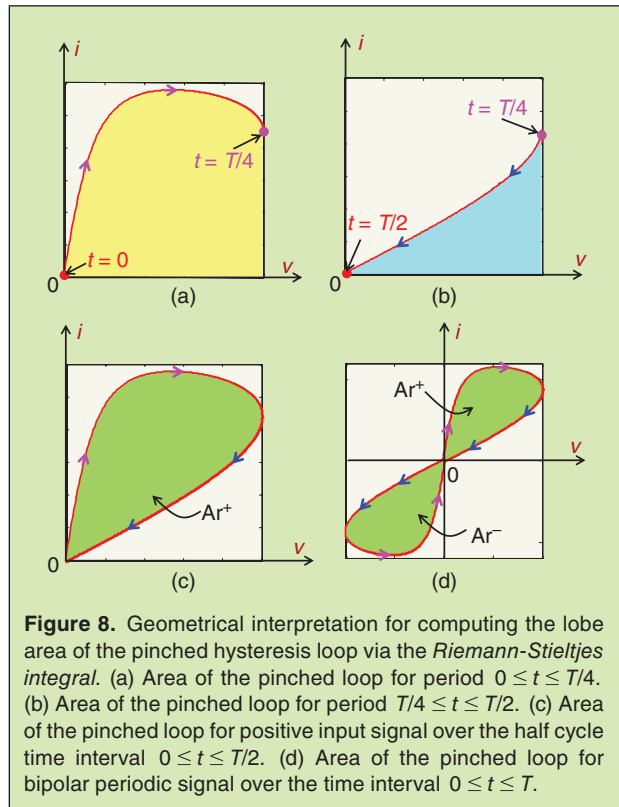


**Figure 8.** Geometrical interpretation for computing the lobe area of the pinched hysteresis loop via the *Riemann–Stieltjes integral*. (a) Area of the pinched loop for period  $0 \leq t \leq T/4$ . (b) Area of the pinched loop for period  $T/4 \leq t \leq T/2$ . (c) Area of the pinched loop for positive input signal over the half cycle time interval  $0 \leq t \leq T/2$ . (d) Area of the pinched loop for bipolar periodic signal over the time interval  $0 \leq t \leq T$ .

Similarly, the 3rd quadrant lobe area ( $Ar^-$ ) of the pinched hysteresis loop for second half cycle  $T/2 \leq t \leq T$  is given by the *Riemann–Stieltjes Integral*,

$$Ar^- = \int_{T/2}^T i(t) \frac{dv(t)}{dt} dt. \quad (8)$$

The 1st and 3rd quadrant lobe area defined by (7) and (8) are illustrated in Fig. 8(d) for one cycle of the bipolar periodic input signal.

Observe that the advantage of using the *Riemann–Stieltjes integral*, and not the conventional *Riemann integral* is that we don't need the formula describing the  $i$ - $v$  curve over different time intervals and we don't have to break up the integration into several parts. The *Riemann–Stieltjes integral* tracks the orientation of the loci and add or subtract the component areas automatically,

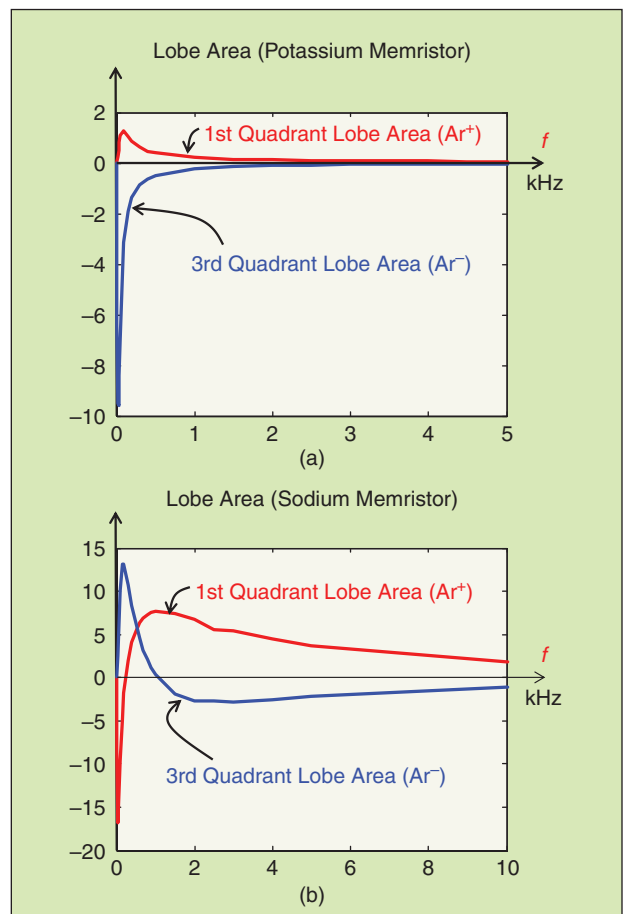


**Figure 9.** Lobe area vs. frequency curve of the potassium and sodium ion channel memristors. (a) The absolute value of lobe area  $|Ar^+|$  and  $|Ar^-|$  of the potassium memristor decreases as the frequency of the input signal increases for  $f > 0.1\text{KHz}$  in the 1st quadrant and for  $f > 0.03\text{ KHz}$  in the 3rd quadrant. (b) The absolute value of the lobe area  $|Ar^+|$  and  $|Ar^-|$  of the sodium memristor decreases as the frequency of the input signal increases for  $f > 1\text{KHz}$  in the 1st quadrant and for  $f > 0.2\text{ KHz}$  in the 3rd quadrant.

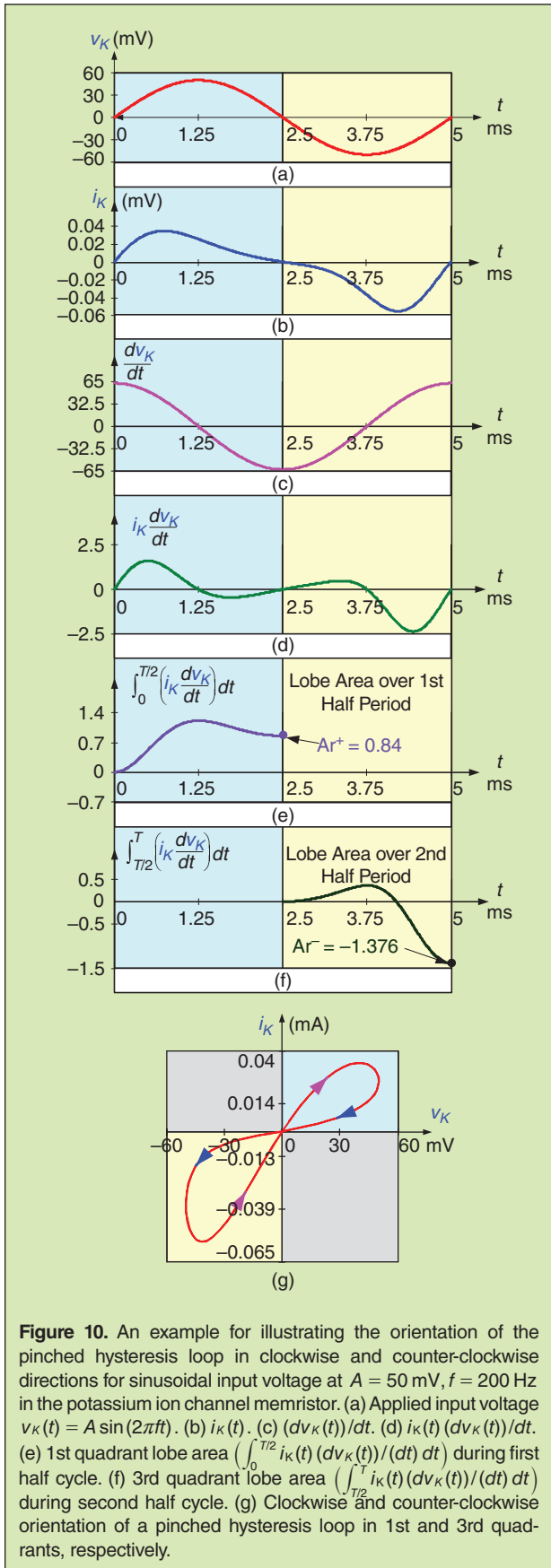


**Figure 10.** An example for illustrating the orientation of the pinched hysteresis loop in clockwise and counter-clockwise directions for sinusoidal input voltage at  $A = 50$  mV,  $f = 200$  Hz in the potassium ion channel memristor. (a) Applied input voltage  $v_K(t) = A \sin(2\pi ft)$ . (b)  $i_K(t)$ . (c)  $(dv_K(t))/dt$ . (d)  $i_K(t) (dv_K(t))/dt$ . (e) 1st quadrant lobe area  $(\int_0^{T/2} i_K(t) ((dv_K(t))/dt) dt)$  during first half cycle. (f) 3rd quadrant lobe area  $(\int_{T/2}^T i_K(t) ((dv_K(t))/dt) dt)$  during second half cycle. (g) Clockwise and counter-clockwise orientation of a pinched hysteresis loop in 1st and 3rd quadrants, respectively.

over the half period  $0 \leq t \leq T/2$ , and  $T/2 \leq t \leq T$ , respectively given only  $i(t)$  and  $dv(t)/dt$ .

We have used the *Riemann-Stieltjes integral* to derive the frequency-dependent characteristic of the lobe area  $Ar^+$  and  $Ar^-$  of the potassium ion-channel and the sodium ion-channel memristors. Fig. 9(a) and Fig. 9(b) show the lobe area *vs. frequency* curve of the potassium and the sodium ion-channel memristor, for input voltage  $v_k = A \sin(2\pi ft)$  and  $v_{Na} = A \sin(2\pi ft)$  with amplitude 50 mV and 120 mV, respectively. As shown in the Fig. 9(a) and Fig. 9(b), the absolute value of the lobe area decreases as the frequency of the input signal increases for  $f > f_c$ . Since the lobe area of the pinched hysteresis loops decreases monotonically with increasing frequency for  $f > f_c$ , the potassium and sodium ion channel memristors exhibit the predicted signature property of a memristor.

#### D. Clockwise and Counter-Clockwise Orientation of the Pinch Hysteresis Loop of a Memristor

The orientation of the pinch hysteresis loop in the 1st or 3rd quadrant of a memristor can occur in a clockwise or counter-clockwise direction with respect to the motion of the tip of a radial vector anchored at the origin. The 1st quadrant pinched hysteresis loop in Fig. 8(c) is oriented in a clockwise direction. The actual area of the lobe is computed by subtracting the area of Fig. 8(b) (Eq. (6)) from the area of Fig. 8(a) (Eq. (5)). Since, the area of Fig. 8(a) is bigger than the area of Fig. 8(b), the actual area of the lobe obtained in the 1st quadrant is positive during first half cycle of a positive input signal. Similarly, the orientation of the pinched hysteresis loop in the 3rd quadrant during second half cycle for a negative input is counter-clockwise.

Let us illustrate the orientation of the pinch hysteresis loop of the potassium and sodium ion channel memristors for a sinusoidal input signal. Fig. 10(a) shows the applied input voltage  $v_K(t) = A \sin(2\pi ft)$  across the potassium ion channel memristor with amplitude  $A = 50$  mV, frequency  $f = 200$  Hz, over a one cycle period  $0 \leq t \leq T$ . Figs. 10(b)–(g) are the corresponding output current  $i_K(t)$ ,  $(dv_K(t))/dt$ ,  $i_K(t) (dv_K(t))/dt$ , 1st quadrant lobe area  $(\int_0^{T/2} i_K(t) ((dv_K(t))/dt) dt)$ , 3rd quadrant lobe area  $(\int_{T/2}^T i_K(t) ((dv_K(t))/dt) dt)$ , and the pinched hysteresis loop, respectively. Observe from Fig. 10(e) and Fig. 10(f) that the 1st and 3rd quadrant lobe area during the first half cycle  $0 \leq t \leq T/2$  and the second half period  $T/2 \leq t \leq T$  are equal to  $Ar^+ = 0.84$  and  $Ar^- = -1.376$ , respectively. The areas of Fig. 10(e) and Fig. 10(f) clearly illustrate that, the orientation of the pinched loop in the 1st quadrant and the 3rd quadrant during the 1st and the 2nd half cycles are clockwise and counter-clockwise, respectively, as shown in Fig. 10(g).

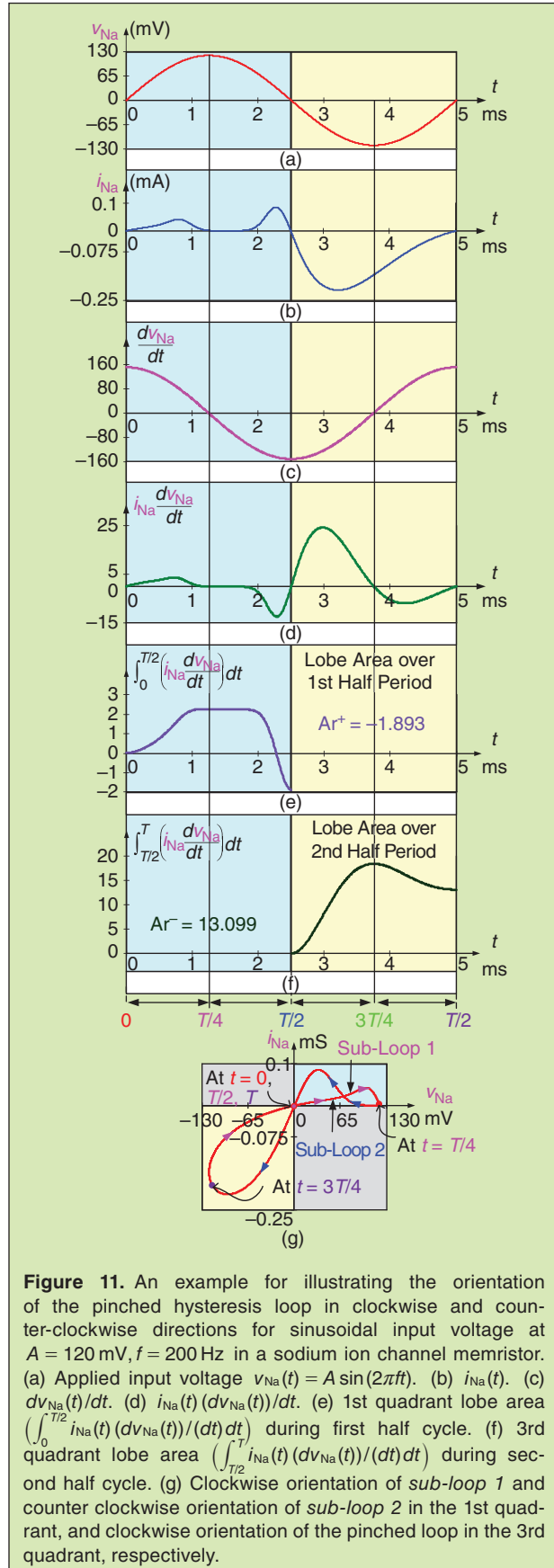
We have also analyzed the orientation of the multi component pinched hysteresis loop of the sodium ion-channel memristor by applying a sinusoidal voltage  $v_{Na}(t) = A \sin(2\pi ft)$ , with amplitude  $A = 120$  mV and frequency  $f = 200$  Hz for one cycle period  $0 \leq t \leq T$ . The input voltage and the corresponding output current  $i_{Na}(t)$ ,  $(dv_{Na}(t))/dt$ ,  $i_{Na}(t)(dv_{Na}(t))/dt$ , 1st quadrant lobe area  $(\int_0^{T/2} i_{Na}(t)(dv_{Na}(t))/(dt) dt)$ , 3rd quadrant lobe area  $(\int_{T/2}^T i_{Na}(t)(dv_{Na}(t))/(dt) dt)$ , and the pinched hysteresis loop, are shown in Figs. 11(a)–(g), respectively. Observe from Fig. 11(e) that the area of the lobe during  $0 \leq t \leq T/4$  is varied from zero to a positive value equal to 2.25. Therefore, the sub-loop during this period is clockwise as indicated in Fig. 11(g), which is named *sub-loop 1*. The area of the lobe during period  $T/4 \leq t \leq T/2$  changes from a positive to a negative value and ends in the negative  $Ar^+$  region at  $Ar^+ = -1.893 < 0$ . Thus the area of the lobe during this period is counter-clockwise as indicated in Fig. 11(g) which is named *sub-loop 2*. The area of the lobe during the second half cycle  $T/2 \leq t \leq T$  changes only in positive direction and ends at the positive region at  $Ar^- = 13.099 > 0$ . Since,  $Ar^-$  is positive, it clearly illustrates the orientation of the pinched hysteresis loop in the 3rd quadrant is clockwise as shown in Fig. 11(g).

In summary we can say that, if the lobe area during a half cycle of the input signal is positive (resp., negative) then the orientation of the pinched loop is clockwise (resp., counter-clockwise) either in the 1st quadrant, or the 3rd quadrant, respectively and vice versa. Table 1 and Table 2 show examples of the computed lobe area and orientation of the pinched hysteresis loops, when the potassium and sodium ion-channel memristors are driven by a sinusoidal voltage source with amplitude 50 mV and 120 mV, respectively, for various frequencies. Table 1 and 2 clearly show the orientations of all the pinched hysteresis loops are clockwise if  $Ar^+ > 0$  and counterclockwise if  $Ar^- < 0$  and vice versa.

### III. DC V-I Curves of the Potassium Ion-Channel Memristor, Sodium Ion-Channel Memristor and Memristive Hodgkin-Huxley Axon Circuit Model

The DC  $V$ - $I$  characteristics of the voltage-dependent potassium and sodium ion channel memristors are obtained by solving their associated state equations for the equilibrium points and substituting the numerically solved values into (3) and (4) for  $i_K$  and  $i_{Na}$ , respectively. The resulting loci of all points  $(V_K, I_K)$  and  $(V_{Na}, I_{Na})$  are called the DC  $V_K$ - $I_K$  and DC  $V_{Na}$ - $I_{Na}$  curves of the potassium and the sodium ion-channel memristors, respectively.

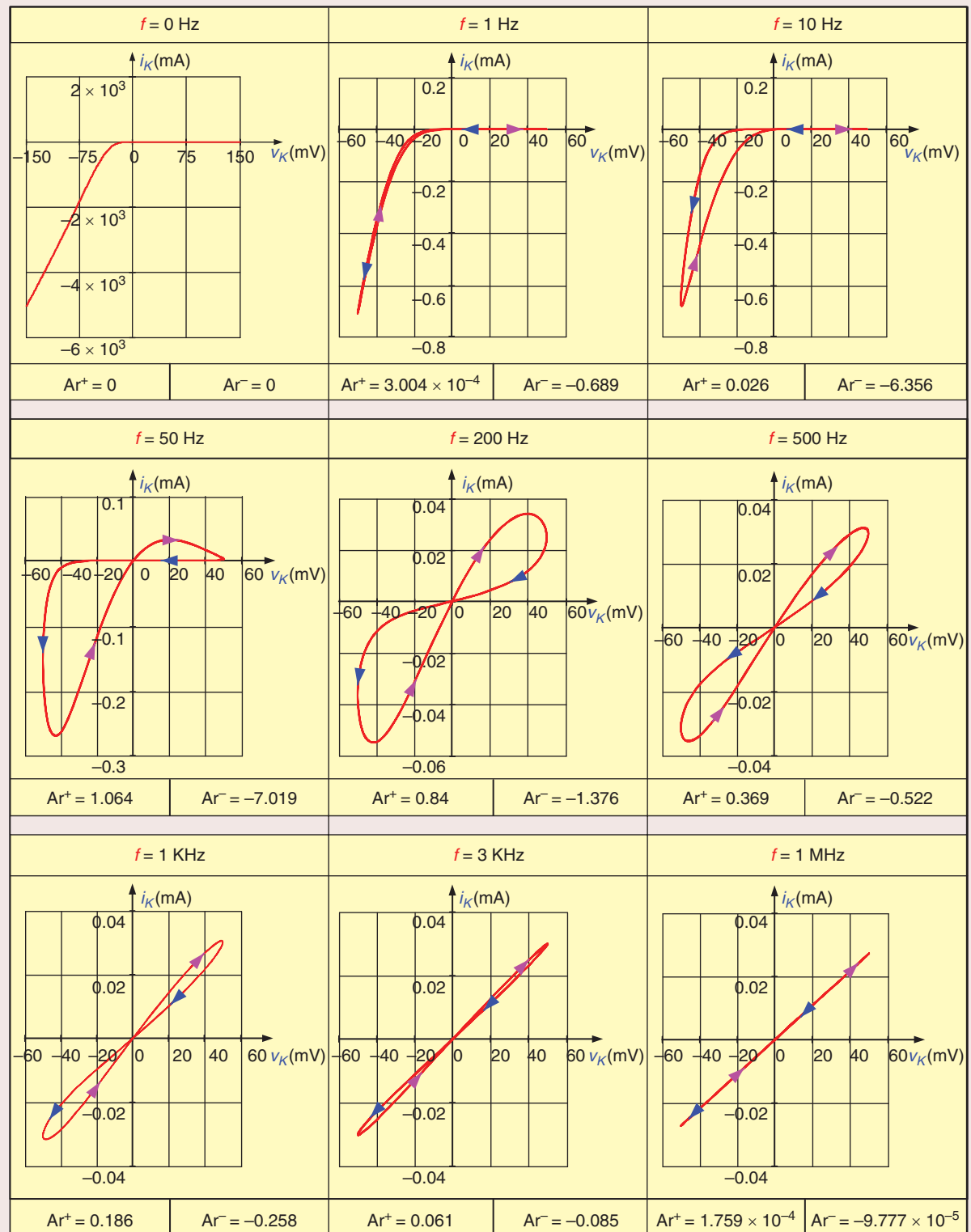
Fig. 12(a) shows the DC  $V_K$ - $I_K$  curve of the potassium ion-channel memristor when the above procedure is



**Figure 11.** An example for illustrating the orientation of the pinched hysteresis loop in clockwise and counter-clockwise directions for sinusoidal input voltage at  $A = 120$  mV,  $f = 200$  Hz in a sodium ion channel memristor. (a) Applied input voltage  $v_{Na}(t) = A \sin(2\pi ft)$ . (b)  $i_{Na}(t)$ . (c)  $(dv_{Na}(t))/dt$ . (d)  $i_{Na}(t)(dv_{Na}(t))/dt$ . (e) 1st quadrant lobe area  $(\int_0^{T/2} i_{Na}(t)(dv_{Na}(t))/(dt) dt)$  during first half cycle. (f) 3rd quadrant lobe area  $(\int_{T/2}^T i_{Na}(t)(dv_{Na}(t))/(dt) dt)$  during second half cycle. (g) Clockwise orientation of *sub-loop 1* and counter-clockwise orientation of *sub-loop 2* in the 1st quadrant, and clockwise orientation of the pinched loop in the 3rd quadrant, respectively.

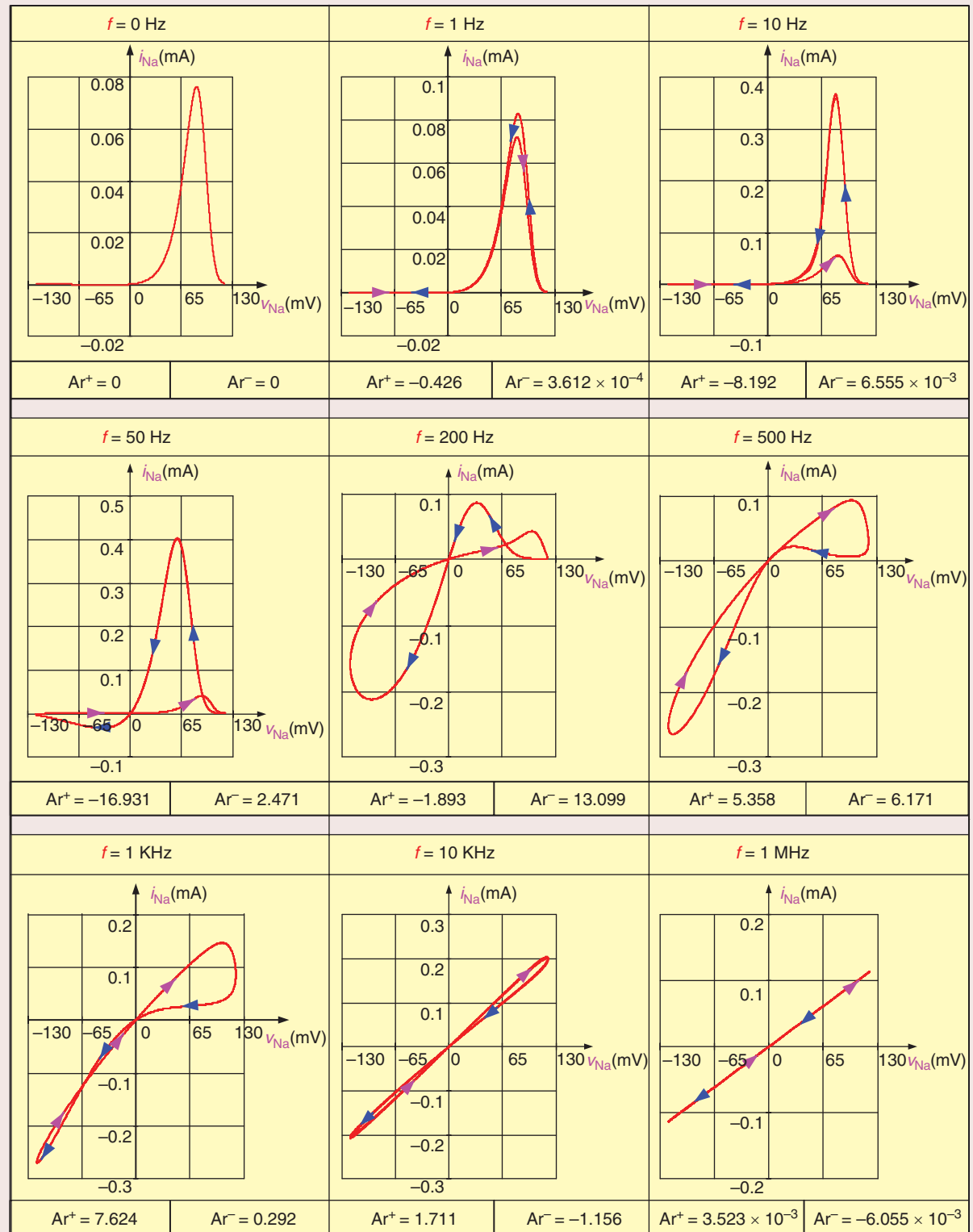
**Table 1.**

Lobe area and orientation of the pinched hysteresis loops of the potassium ion-channel memristor for input voltage  $v_K(t) = A \sin(2\pi ft)$  with amplitude  $A = 50$  mV.



**Table 2.**

Lobe area and orientation of the pinched hysteresis loops of the sodium ion-channel memristor for input voltage  $v_{Na}(t) = A \sin(2\pi ft)$  with amplitude  $A = 120$  mV.



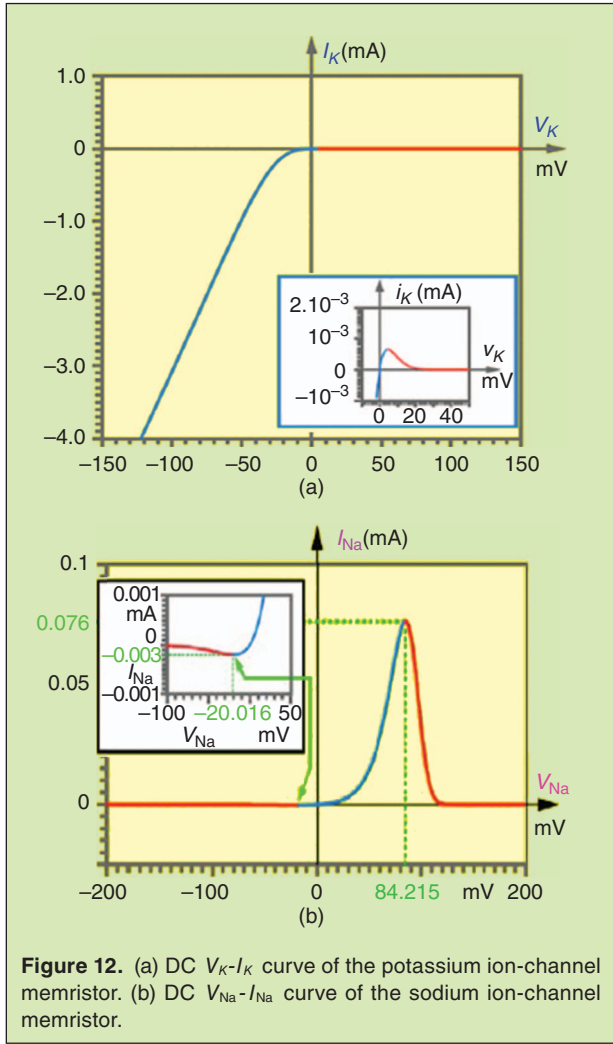


**Figure 12.** (a) DC  $V_K$ - $I_K$  curve of the potassium ion-channel memristor. (b) DC  $V_{Na}$ - $I_{Na}$  curve of the sodium ion-channel memristor.

applied over the range of input voltage  $-150 \text{ mV} \leq V_K \leq 150 \text{ mV}$ . The right bottom inset shows the magnified plot of the  $V_K$ - $I_K$  curve over  $0 \leq V_K \leq 50 \text{ mV}$ . The positive and negative slopes of the DC  $V_K$ - $I_K$  curve are printed in blue and red, respectively. Similarly, by applying above procedure to the sodium ion channel memristor, we obtain the DC  $V_{Na}$ - $I_{Na}$  curve shown in Fig. 12(b) over the range  $-200 \text{ mV} \leq V_{Na} \leq 200 \text{ mV}$ . The upper-left inset is the enlargement of the DC  $V_{Na}$ - $I_{Na}$  curve over  $-100 \text{ mV} \leq V_{Na} \leq 50 \text{ mV}$ . Note that the positive and negative slopes of the DC  $V_{Na}$ - $I_{Na}$  curve are printed in blue and red, respectively.

The points  $(V_K, I_K)$  on the red portion of the potassium DC  $V_K$ - $I_K$  curve are *locally-active* [10] in the sense that it is possible to imbed the memristor in a passive circuit which *amplifies* the power of a small input signal and produces an output signal with a larger power, at the expense of an informationless DC power supply, namely, the battery used to bias the potassium

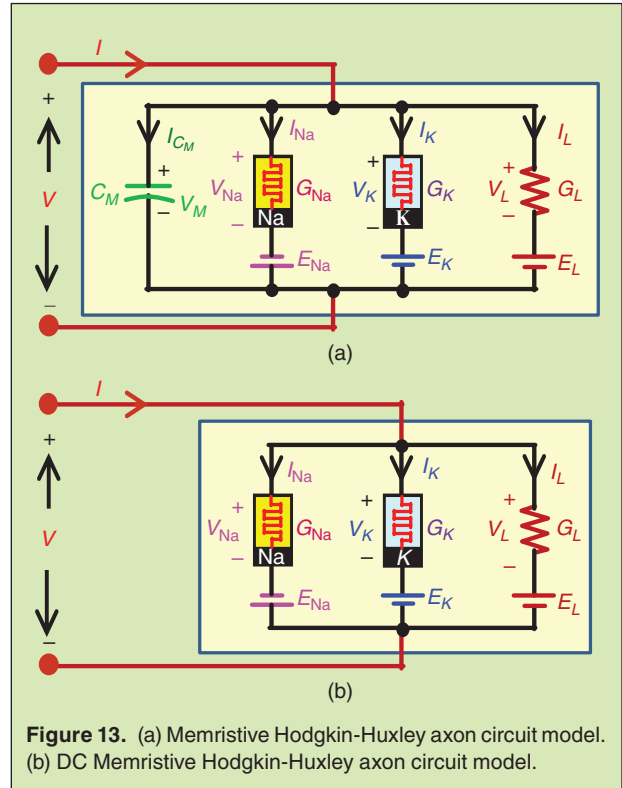


**Figure 13.** (a) Memristive Hodgkin-Huxley axon circuit model. (b) DC Memristive Hodgkin-Huxley axon circuit model.

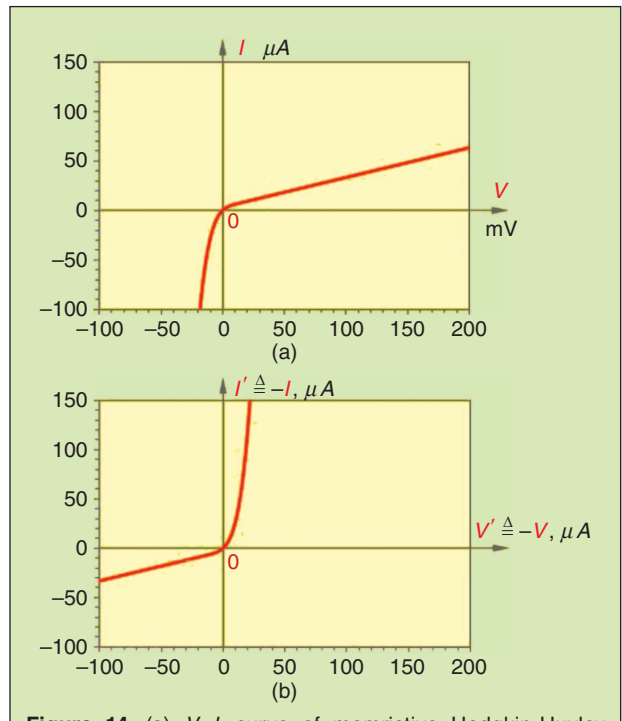


**Figure 14.** (a)  $V$ - $I$  curve of memristive Hodgkin-Huxley axon circuit model. (b)  $180^\circ$ -rotated  $V$ - $I$  curve from (a) where  $V'$  and  $I'$  are corresponding voltage and current variables defined with modern reference convention.

memristor at the prescribed DC equilibrium point. Similarly, the points  $(V_{\text{Na}}, I_{\text{Na}})$  on the red portion of the DC  $V_{\text{Na}}-I_{\text{Na}}$  curve are locally active.

The memristive Hodgkin-Huxley axon circuit model is reproduced from [5] and shown in Fig. 13(a). The DC equivalent circuit obtained by deleting the capacitor  $C_M$  is shown in Fig. 13(b).

The DC  $V$ - $I$  curve of the memristive Hodgkin-Huxley axon circuit model was derived in [5] and reproduced in Fig. 14(a). For ease of the comparison with the modern reference convention in the literature on Hodgkin-Huxley axon circuit model, which is the *reverse* of those originally adopted by Hodgkin and Huxley in their classic 1952 paper [4], we have also plotted the corresponding DC  $V'$ - $I'$  curve in Fig. 14(b) using the modern reference convention where  $V' \triangleq -V$  and  $I' \triangleq -I$ . Note that this DC  $V'$ - $I'$  curve resembles that of the *vacuum diode*, and the *pn junction*, which explains and resolves the “rectifier” anomaly that had mystified many distinguished physiologists including Hodgkin and Cole [11].

We remark that a “negative slope” on the DC  $V$ - $I$  curve of a memristor is only a *sufficient* condition for local activity. An equilibrium point on a DC  $V$ - $I$  curve of a memristor with a *positive slope* can also be *locally*

*active* if  $\text{Re}Y_K(f; V_K(Q)) < 0$  for the potassium memristor, and  $\text{Re}Y_{\text{Na}}(f; V_{\text{Na}}(Q)) < 0$  for the sodium memristor at some frequency  $f = f_0$  [12]. A memristor is defined to be *locally active* if there exists at least one DC equilibrium point  $Q$  where it is *locally active*. It follows that both the potassium memristor and sodium memristor are *locally active*.

#### IV. Small-Signal Equivalent Circuits and Nyquist Plot of Ion-Channel Memristor

Small-signal equivalent circuits of ion-channel memristors are fundamental concepts and tools for predicting the nonlinear dynamics of the Hodgkin-Huxley axon. Applying standard circuit analysis method [5], we can derive the small-signal equivalent circuit about *each* DC equilibrium point  $(V_K, I_K)$  for the potassium ion-channel memristor, and  $(V_{\text{Na}}, I_{\text{Na}})$  for the sodium ion-channel memristor. We can then derive the admittance  $Y_K(s, Q_K)$  for the potassium memristor, and  $Y_{\text{Na}}(s, Q_{\text{Na}})$  for the sodium memristor.

In this section, we analyze the small-signal equivalent circuits and the Nyquist plot of the potassium ion-channel memristor, the sodium-ion channel memristor and the memristive Hodgkin-Huxley axon circuit model.

**Table 3.**  
Explicit Equations for  $L(K)$ ,  $R_1(K)$ , and  $R_2(K)$  as functions of  $V_K$ .

$$L(K) = \frac{1}{c_n b_n}$$

$$c_n(V_K) = 4\bar{g}_K n(V_K)^3 V_K,$$

$$b_n(V_K) = 0.01(n(V_K) - 1) \left( \frac{(V_K + E_K + 10)e^{(V_K + E_K + 10)/10}}{10(e^{(V_K + E_K + 10)/10} - 1)^2} - \frac{1}{(e^{(V_K + E_K + 10)/10} - 1)} \right) - 0.125n(V_K) \frac{e^{(V_K + E_K)/80}}{80},$$

$$R_1(K) = \frac{\alpha_n + \beta_n}{c_n b_n}$$

$$\alpha_n(V_K) = \frac{0.01(V_K + E_K + 10)}{\exp\{(V_K + E_K + 10)/10\} - 1},$$

$$\beta_n(V_K) = 0.125 \exp\{(V_K + E_K)/80\},$$

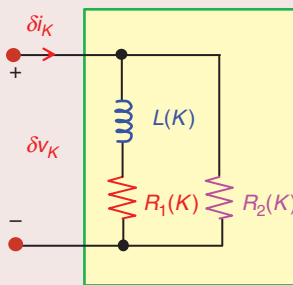
$$R_2(K) = \frac{1}{d_K}$$

$$d_K = \bar{g}_K n(V_K)^4,$$

$$n(V_K) = \frac{\alpha_n(V_K)}{\alpha_n(V_K) + \beta_n(V_K)},$$

$$E_K = 12 \text{ mV}, \quad \bar{g}_K = 36 \text{ mS}$$

Potassium Ion-Channel Memristor Small-Signal Equivalent Circuit at Equilibrium Point  $V_K(Q)$



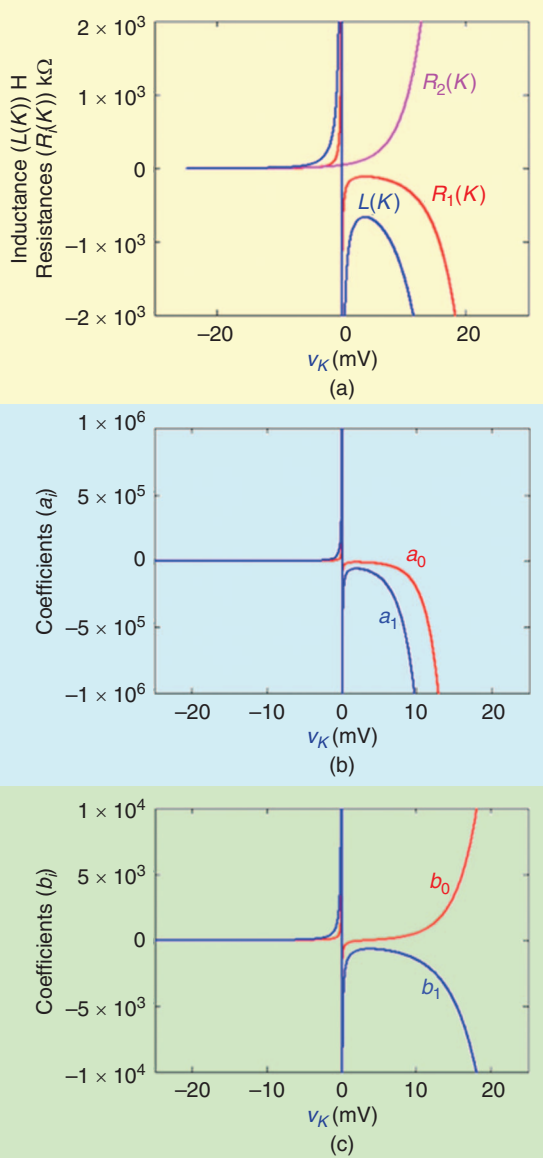


**Figure 15.** (a) Variation of the inductance  $L(K)$ , resistance  $R_1(K)$  and resistance  $R_2(K)$  as a function of the potassium ion-channel memristor at the DC equilibrium voltage  $V_K$  (b) Variation of the coefficients  $a_0, a_1$  as a function of the potassium ion-channel memristor at the DC equilibrium voltage  $V_K$ . (c) Variation of the coefficients  $b_0, b_1$  as a function of the potassium ion-channel memristor at the DC equilibrium voltage  $V_K$ .

#### A. Small-Signal Equivalent Circuit and Nyquist Plot of the Potassium Ion-Channel Memristor

The small-signal equivalent circuit of the potassium ion-channel memristor was derived in [5] and reproduced in Table 3. Observe that the values of the three circuit elements  $L(K), R_1(K)$  and  $R_2(K)$  about each DC equilibrium point at  $(V_K(Q_K), I_K(Q_K))$  can be calculated via the explicit formulas given in Table 3.

The admittance of the small-signal equivalent circuit of the potassium ion-channel memristor about an equilibrium point  $Q_K$  is given by [5]

$$Y_K(s, Q_K) = \frac{1}{sL(K) + R_1(K)} + \frac{1}{R_2(K)}. \quad (9)$$

We can recast (9) as a rational function of  $s$ :

$$Y_K(s, Q_K) = \frac{b_1(K)s + b_0(K)}{a_1(K)s + a_0(K)}, \quad (10a)$$

where

$$a_0(K) = R_1(K)R_2(K), a_1(K) = L(K)R_2(K) \quad (10b)$$

$$b_0(K) = R_1(K) + R_2(K), b_1(K) = L(K). \quad (10c)$$

The explicit formula for calculating the inductance  $L(K)$ , and resistances  $R_1(K)$  and  $R_2(K)$  are given in Table 3 as function of  $V_K$  at the DC equilibrium point  $Q_K$ .

Substituting  $s = i\omega = i(2\pi f)$  for the complex frequency  $s$  in (10a), we obtain small-signal admittance function  $Y_K(f; V_K)$  of the potassium ion-channel at the DC equilibrium point  $v_K = V_K(Q_K)$ . The real and imaginary parts of  $Y_K(f; V_K)$  as a function of the frequency  $f$  is given by

$$Y_K(f, V_K) = \left[ \frac{(a_0 b_0 + a_1 b_1 (2\pi f)^2)}{(a_0^2 + a_1^2 (2\pi f)^2)} \right] + i \left[ \frac{(a_0 b_1 - a_1 b_0)(2\pi f)}{(a_0^2 + a_1^2 (2\pi f)^2)} \right]. \quad (11a)$$

Here the symbol  $K$  attached to the coefficients  $a_i$  and  $b_i$  is deleted to avoid clutter. Hence,

$$\text{Re } Y_K(f, V_K) = \frac{a_0 b_0 + a_1 b_1 (2\pi f)^2}{a_0^2 + a_1^2 (2\pi f)^2} \quad (11b)$$

and

$$\text{Im } Y_K(f, V_K) = \frac{(a_0 b_1 - a_1 b_0)(2\pi f)}{a_0^2 + a_1^2 (2\pi f)^2}. \quad (11c)$$

The small-signal equivalent circuit of the potassium ion-channel memristor shown in Table 3 is composed of one inductance and two resistances respectively. The parameters of the small-signal equivalent circuits and the value of the coefficients depend on  $v_K = V_K(Q_K)$  at the equilibrium point  $Q_K$ . The variation of the inductance  $L(K)$ , resistances  $R_1(K)$  and  $R_2(K)$ , coefficients  $a_0, a_1$  and coefficients  $b_0, b_1$  of the small-signal potassium admittance function defined in (9) and (10) are shown in Figs. 15(a), (b) and (c), respectively, as a function of the DC potassium ion-channel memristor voltage  $V_K$ .

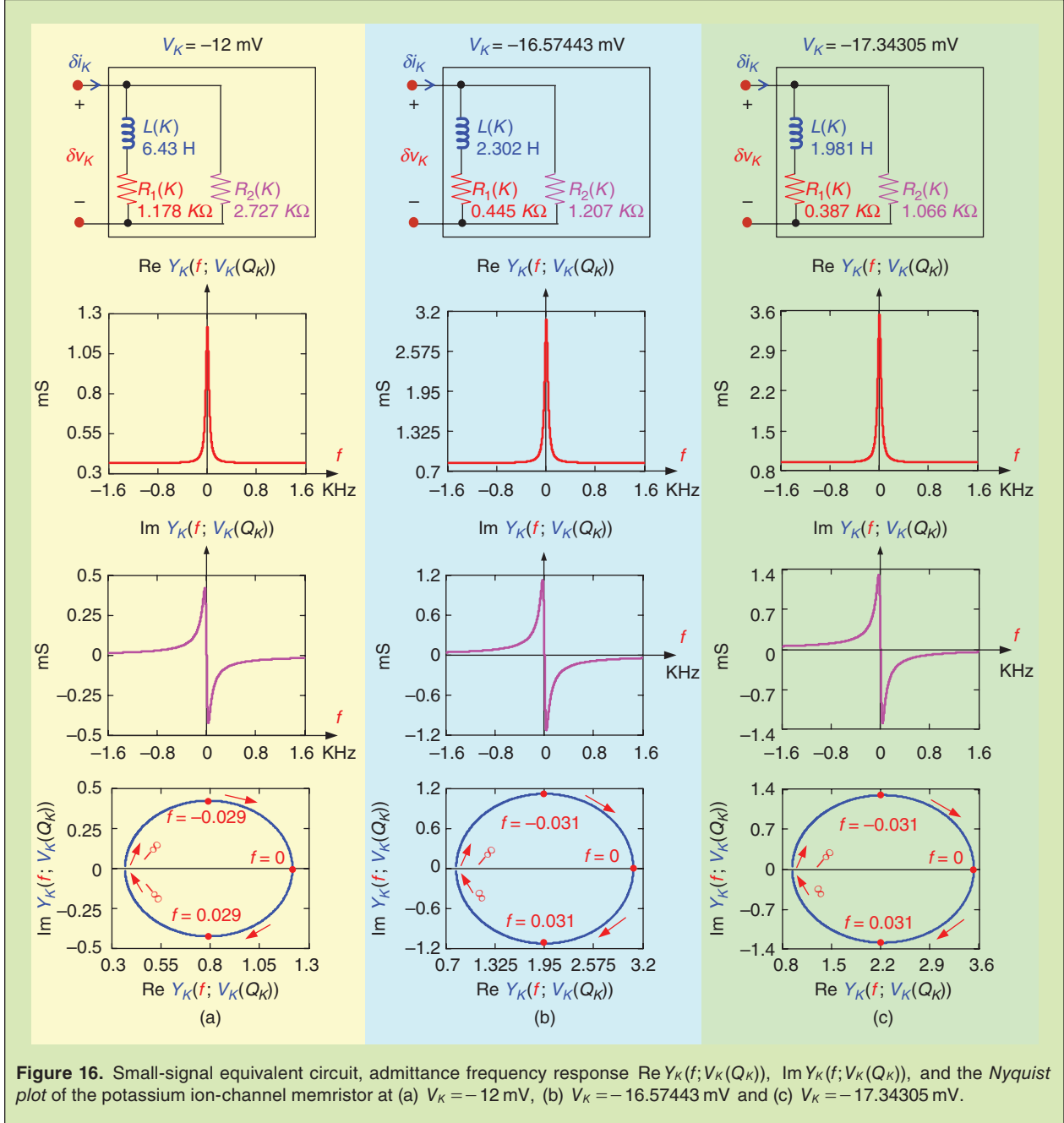


**Figure 16.** Small-signal equivalent circuit, admittance frequency response  $\text{Re } Y_K(f; V_K(Q_K))$ ,  $\text{Im } Y_K(f; V_K(Q_K))$ , and the Nyquist plot of the potassium ion-channel memristor at (a)  $V_K = -12 \text{ mV}$ , (b)  $V_K = -16.57443 \text{ mV}$  and (c)  $V_K = -17.34305 \text{ mV}$ .

The real part  $\text{Re } Y_K(f; V_K)$  and imaginary part  $\text{Im } Y_K(f; V_K)$  obtained from the potassium admittance function  $Y_K(f; V_K)$  is called the small-signal admittance *frequency response* of the potassium ion-channel at equilibrium point  $v_K = V_K(Q_K)$ . When, the real part  $\text{Re } Y_K(f; V_K)$  and imaginary part  $\text{Im } Y_K(f; V_K)$  of the admittance function of  $Y_K(f; V_K)$  are plotted on the horizontal and vertical axes of the Cartesian coordinate system with the frequency  $f$  as a parameter, the resulting plot is generally called the *Nyquist plot* of the

admittance  $Y_K(f; V_K)$ . Figs. 16(a), (b) and (c) show the small-signal *equivalent circuit*, small-signal admittance *frequency response*  $Y_K(f; V_K) = \text{Re } Y_K(f; V_K) + \text{Im } Y_K(f; V_K)$ , and the *Nyquist plot* of the potassium ion-channel memristor at  $V_K = -12 \text{ mV}$ ,  $V_K = -16.57443 \text{ mV}$  and  $V_K = -17.34305 \text{ mV}$ , respectively. These three voltages are chosen to correspond to the three equilibrium voltages  $V_m = 0$ ,  $V_m = -4.57443 \text{ mV}$ , and  $V_m = -5.34305 \text{ mV}$  of the DC memristive Hodgkin-Huxley axon circuit model.

**Table 4.**  
Explicit Equations for  $L_1(\text{Na})$ ,  $R_1(\text{Na})$ ,  $L_2(\text{Na})$ ,  $R_2(\text{Na})$  and  $R_3(\text{Na})$  as functions of  $V_{\text{Na}}$ .

$$L_1(\text{Na}) = \frac{1}{C_m b_m} \quad C_m(V_{\text{Na}}) = 3\bar{g}_{\text{Na}} m(V_{\text{Na}})^2 h(V_{\text{Na}}) V_{\text{Na}},$$

$$b_m(V_{\text{Na}}) = 0.1(m(V_{\text{Na}}) - 1)$$

$$\left( \frac{(V_{\text{Na}} - E_{\text{Na}} + 25) e^{(V_{\text{Na}} - E_{\text{Na}} + 25)/10}}{10(e^{(V_{\text{Na}} - E_{\text{Na}} + 25)/10} - 1)^2} - \frac{1}{(e^{(V_{\text{Na}} - E_{\text{Na}} + 25)/10} - 1)} \right)$$

$$- 4m(V_{\text{Na}}) \frac{e^{(V_{\text{Na}} - E_{\text{Na}})/18}}{18},$$

$$L_2(\text{Na}) = \frac{1}{C_h b_h} \quad C_h(V_{\text{Na}}) = \bar{g}_{\text{Na}} m(V_{\text{Na}})^3 V_{\text{Na}},$$

$$b_h(V_{\text{Na}}) = \frac{h(V_{\text{Na}}) e^{(V_{\text{Na}} - E_{\text{Na}} + 30)/10}}{10(e^{(V_{\text{Na}} - E_{\text{Na}} + 30)/10} + 1)^2}$$

$$- 0.07(h(V_{\text{Na}}) - 1) \frac{e^{(V_{\text{Na}} - E_{\text{Na}})/20}}{20}$$

$$R_1(\text{Na}) = \frac{\alpha_m + \beta_m}{c_m + b_m} \quad \alpha_m(V_{\text{Na}}) = \frac{0.1(V_{\text{Na}} - E_{\text{Na}} + 25)}{\exp\{(V_{\text{Na}} - E_{\text{Na}} + 25)/10\} - 1},$$

$$\beta_m(V_{\text{Na}}) = 4\exp\{(V_{\text{Na}} - E_{\text{Na}})/18\},$$

$$R_2(\text{Na}) = \frac{\alpha_h + \beta_h}{c_h b_h} \quad \alpha_h(V_{\text{Na}}) = 0.07\exp\{(V_{\text{Na}} - E_{\text{Na}})/20\},$$

$$\beta_h(V_{\text{Na}}) = \frac{1}{\exp\{(V_{\text{Na}} - E_{\text{Na}} + 30)/10\} + 1},$$

$$R_3(\text{Na}) = \frac{1}{d_{\text{Na}}} \quad d_{\text{Na}} = \bar{g}_{\text{Na}} m(V_{\text{Na}})^3 h(V_{\text{Na}}),$$

$$m(V_{\text{Na}}) = \frac{\alpha_m(V_{\text{Na}})}{\alpha_m(V_{\text{Na}}) + \beta_m(V_{\text{Na}})}$$

$$h(V_{\text{Na}}) = \frac{\alpha_h(V_{\text{Na}})}{\alpha_h(V_{\text{Na}}) + \beta_h(V_{\text{Na}})}$$

$$E_{\text{Na}} = 115 \text{ mV}, \bar{g}_{\text{Na}} = 120 \text{ mS}$$

Sodium Ion-Channel  
Memristor Small-Signal  
Equivalent Circuit at  
Equilibrium Point  $V_{\text{Na}}(Q)$

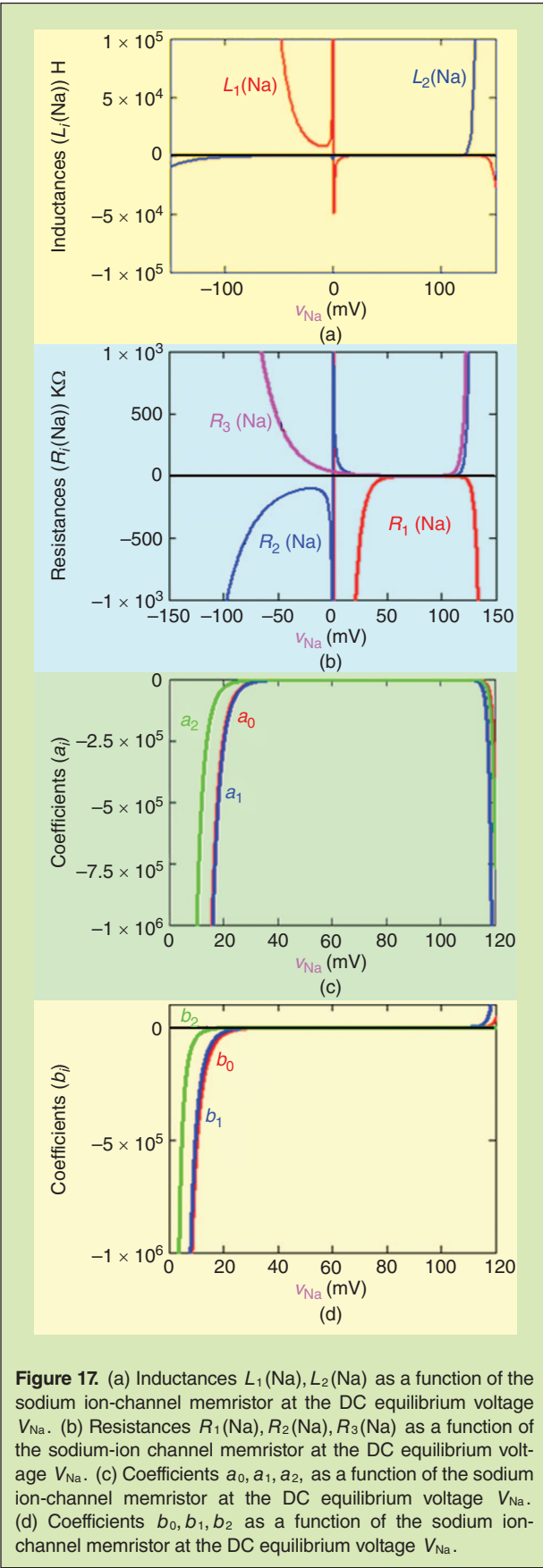
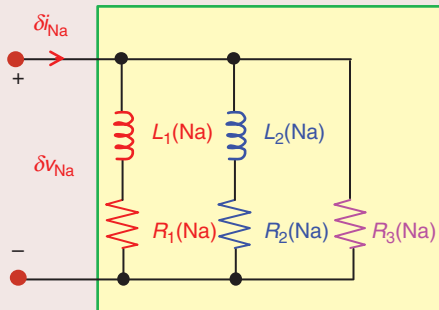


**Figure 17.** (a) Inductances  $L_1(\text{Na}), L_2(\text{Na})$  as a function of the sodium ion-channel memristor at the DC equilibrium voltage  $V_{\text{Na}}$ . (b) Resistances  $R_1(\text{Na}), R_2(\text{Na}), R_3(\text{Na})$  as a function of the sodium-ion channel memristor at the DC equilibrium voltage  $V_{\text{Na}}$ . (c) Coefficients  $a_0, a_1, a_2$ , as a function of the sodium ion-channel memristor at the DC equilibrium voltage  $V_{\text{Na}}$ . (d) Coefficients  $b_0, b_1, b_2$  as a function of the sodium ion-channel memristor at the DC equilibrium voltage  $V_{\text{Na}}$ .

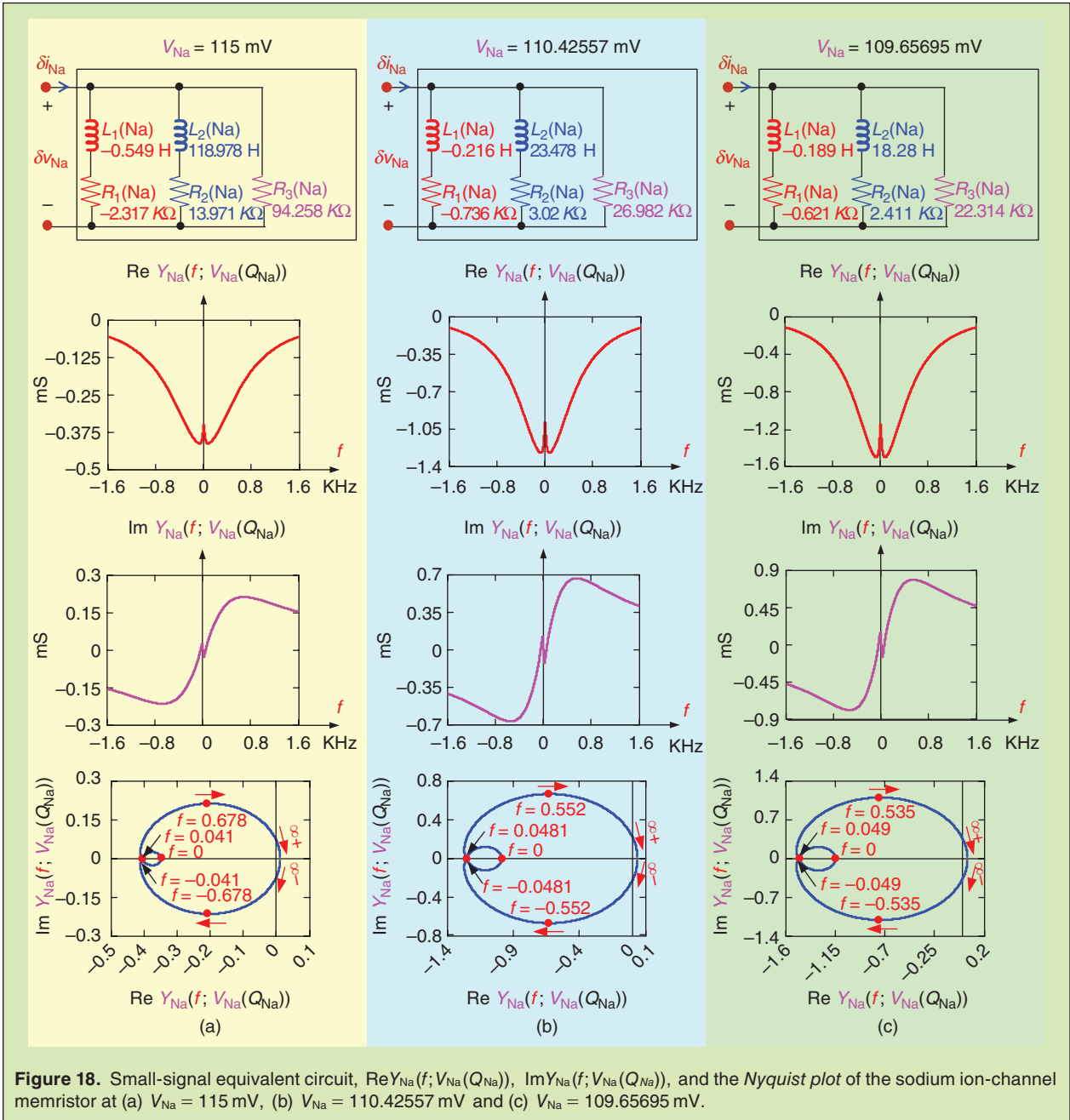


**Figure 18.** Small-signal equivalent circuit,  $\text{Re } Y_{Na}(f; V_{Na}(Q_{Na}))$ ,  $\text{Im } Y_{Na}(f; V_{Na}(Q_{Na}))$ , and the Nyquist plot of the sodium ion-channel memristor at (a)  $V_{Na} = 115 \text{ mV}$ , (b)  $V_{Na} = 110.42557 \text{ mV}$  and (c)  $V_{Na} = 109.65695 \text{ mV}$ .

### B. Small-Signal Equivalent Circuit and Nyquist Plot of the Sodium Ion-Channel Memristor

The small-signal equivalent circuit of the sodium ion-channel memristor was derived in [5] and reproduced in Table 4. Observe that the values of the five circuit elements  $L_1(\text{Na})$ ,  $L_2(\text{Na})$ ,  $R_1(\text{Na})$ ,  $R_2(\text{Na})$  and  $R_3(\text{Na})$  about each DC equilibrium point  $Q_{\text{Na}}$  at  $(V_{Na}(Q_{\text{Na}}), I_{\text{Na}}(Q_{\text{Na}}))$  in Fig. 12(b) can be calculated via the explicit formulas given in Table 4.

The expression for the admittance of the small-signal equivalent circuit of the sodium ion-channel memristor

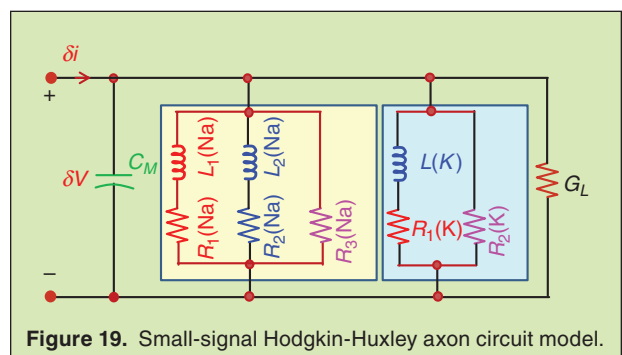


**Figure 19.** Small-signal Hodgkin-Huxley axon circuit model.

**Table 5.**  
**Formulas for calculating coefficients of  $Y(s; V_m)$  of the Hodgkin-Huxley Axon Circuit Model.**

$$\begin{aligned}
 a_0 &= R_1(\text{Na}) R_2(\text{Na}) R_3(\text{Na}) R_1(K) R_2(K) \\
 a_1 &= R_3(\text{Na}) R_2(K) [L(K) R_1(\text{Na}) R_2(\text{Na}) + R_1(K) \{R_1(\text{Na}) L_2(\text{Na}) + R_2(\text{Na}) L_1(\text{Na})\}] \\
 a_2 &= R_3(\text{Na}) R_2(K) [R_1(K) L_1(\text{Na}) L_2(\text{Na}) + L(K) \{R_1(\text{Na}) L_2(\text{Na}) + R_2(\text{Na}) L_1(\text{Na})\}] \\
 a_3 &= R_3(\text{Na}) R_2(K) L_1(\text{Na}) L_2(\text{Na}) L(K) \\
 b_0 &= R_1(K) R_2(K) [R_1(\text{Na}) R_2(\text{Na}) + R_2(\text{Na}) R_3(\text{Na}) + R_3(\text{Na}) R_1(\text{Na})] + R_1(\text{Na}) R_2(\text{Na}) R_3(\text{Na}) [R_1(K) + R_2(K)] \\
 &\quad + R_1(\text{Na}) R_2(\text{Na}) R_3(\text{Na}) R_1(K) R_2(K) G_L \\
 b_1 &= R_3(\text{Na}) [R_1(K) L_2(\text{Na}) R_1(\text{Na}) + R_2(\text{Na}) \{L(K) R_1(\text{Na}) + R_1(K) L_1(\text{Na})\} + R_2(K) \{L_1(\text{Na}) R_2(\text{Na}) + L_2(\text{Na}) R_1(\text{Na})\}] \\
 &\quad + R_3(\text{Na}) R_2(K) [[L(K) R_1(\text{Na}) R_2(\text{Na}) + R_1(K) \{L_1(\text{Na}) R_2(\text{Na}) + L_2(\text{Na}) R_1(\text{Na})\}] G_L + R_1(K) R_1(\text{Na}) R_2(\text{Na}) C_M] \\
 &\quad + L(K) R_2(K) [R_1(\text{Na}) R_2(\text{Na}) + R_2(\text{Na}) R_3(\text{Na}) + R_1(\text{Na}) R_2(\text{Na})] \\
 &\quad + R_1(K) R_2(K) [L_1(\text{Na}) \{R_2(\text{Na}) + R_3(\text{Na})\} + L_2(\text{Na}) \{R_1(\text{Na}) + R_3(\text{Na})\}] \\
 b_2 &= R_2(K) R_3(\text{Na}) \left[ \begin{array}{l} \{(R_1(K) L_1(\text{Na}) L_2(\text{Na}) + L(K) \{R_1(\text{Na}) L_2(\text{Na}) + R_2(\text{Na}) L_1(\text{Na})\})\} G_L \\ + \{L(K) R_1(\text{Na}) R_2(\text{Na}) + R_1(K) \{R_1(\text{Na}) L_2(\text{Na}) + R_2(\text{Na}) L_1(\text{Na})\}\} C_M \end{array} \right] \\
 &\quad + R_3(\text{Na}) [L(K) L_2(\text{Na}) R_1(\text{Na}) + L_1(\text{Na}) \{L(K) R_2(\text{Na}) + L_2(\text{Na}) [R_1(K) + R_2(K)]\}] \\
 &\quad + R_2(K) [L_1(\text{Na}) L_2(\text{Na}) R_1(K) + L(K) \{L_1(\text{Na}) [R_2(\text{Na}) + R_3(\text{Na})] + L_2(\text{Na}) [R_1(\text{Na}) + R_3(\text{Na})]\}] \\
 b_3 &= L_1(\text{Na}) L_2(\text{Na}) L(K) [R_2(K) + R_3(\text{Na})] \\
 &\quad + R_3(\text{Na}) R_2(K) [L_1(\text{Na}) L_2(\text{Na}) L(K) G_L + [R_1(K) L_1(\text{Na}) L_2(\text{Na}) + L(K) \{R_1(\text{Na}) L_2(\text{Na}) + R_2(\text{Na}) L_1(\text{Na})\}] C_M] \\
 b_4 &= R_3(\text{Na}) R_2(K) L_1(\text{Na}) L_2(\text{Na}) L(K) C_M
 \end{aligned}$$

from the Hodgkin-Huxley axon circuit model about an equilibrium point  $Q_{\text{Na}}$  is given by [5]

$$\begin{aligned}
 Y_{\text{Na}}(s, Q_{\text{Na}}) &= \frac{1}{s L_1(\text{Na}) + R_1(\text{Na})} \\
 &\quad + \frac{1}{s L_2(\text{Na}) + R_2(\text{Na})} + \frac{1}{R_3(\text{Na})}. \quad (12)
 \end{aligned}$$

We can recast the admittance function (12) as a *rational function* of  $s$ :

$$Y_{\text{Na}}(s, Q_{\text{Na}}) = \frac{b_2(\text{Na}) s^2 + b_1(\text{Na}) s + b_0(\text{Na})}{a_2(\text{Na}) s^2 + a_1(\text{Na}) s + a_0(\text{Na})}, \quad (13a)$$

where

$$\left. \begin{aligned}
 a_0(\text{Na}) &= R_1(\text{Na}) R_2(\text{Na}) R_3(\text{Na}) \\
 a_1(\text{Na}) &= (L_1(\text{Na}) R_2(\text{Na}) + L_2(\text{Na}) R_1(\text{Na})) R_3(\text{Na}) \\
 a_2(\text{Na}) &= L_1(\text{Na}) L_2(\text{Na}) R_3(\text{Na})
 \end{aligned} \right\} \quad (13b)$$

$$\left. \begin{aligned}
 b_0(\text{Na}) &= R_1(\text{Na}) R_2(\text{Na}) + R_1(\text{Na}) R_3(\text{Na}) \\
 &\quad + R_2(\text{Na}) R_3(\text{Na}) \\
 b_1(\text{Na}) &= L_1(\text{Na}) R_2(\text{Na}) + L_2(\text{Na}) R_1(\text{Na}) \\
 &\quad + L_1(\text{Na}) R_3(\text{Na}) + L_2(\text{Na}) R_3(\text{Na}) \\
 b_2(\text{Na}) &= L_1(\text{Na}) L_2(\text{Na})
 \end{aligned} \right\} \quad (13c)$$

Explicit formulas for calculating  $L_1(\text{Na})$ ,  $R_1(\text{Na})$ ,  $L_2(\text{Na})$ ,  $R_2(\text{Na})$  and  $R_3(\text{Na})$  are given in Table 4, as a function of  $V_{\text{Na}}$  at the DC equilibrium point  $Q_{\text{Na}}$ .

Substituting  $s = i\omega = i(2\pi f)$  in Eq. (13a) and rearranging  $Y_{\text{Na}}(f, V_{\text{Na}})$  into its real and imaginary parts we obtain

$$\begin{aligned}
 Y_{\text{Na}}(f, V_{\text{Na}}) &= \left[ \frac{(a_0 - a_2(2\pi f)^2)(b_0 - b_2(2\pi f)^2) + a_1 b_1(2\pi f)^2}{(a_0 - a_2(2\pi f)^2)^2 + a_1^2(2\pi f)^2} \right] \\
 &\quad + i \left[ \frac{[(a_0 - a_2(2\pi f)^2)b_1 - a_1(b_0 - b_2(2\pi f)^2)](2\pi f)}{(a_0 - a_2(2\pi f)^2)^2 + a_1^2(2\pi f)^2} \right], \quad (14a)
 \end{aligned}$$

where we have deleted the symbol Na attached to the coefficients  $a_i$  and  $b_i$  to avoid clutter. Hence,

$$\text{Re } Y_{\text{Na}}(f, V_{\text{Na}}) = \frac{(a_0 - a_2(2\pi f)^2)(b_0 - b_2(2\pi f)^2) + a_1 b_1(2\pi f)^2}{(a_0 - a_2(2\pi f)^2)^2 + a_1^2(2\pi f)^2} \quad (14b)$$

and

$$\text{Im } Y_{\text{Na}}(f, V_{\text{Na}}) = \frac{[(a_0 - a_2(2\pi f)^2)b_1 - a_1(b_0 - b_2(2\pi f)^2)](2\pi f)}{(a_0 - a_2(2\pi f)^2)^2 + a_1^2(2\pi f)^2}. \quad (14c)$$

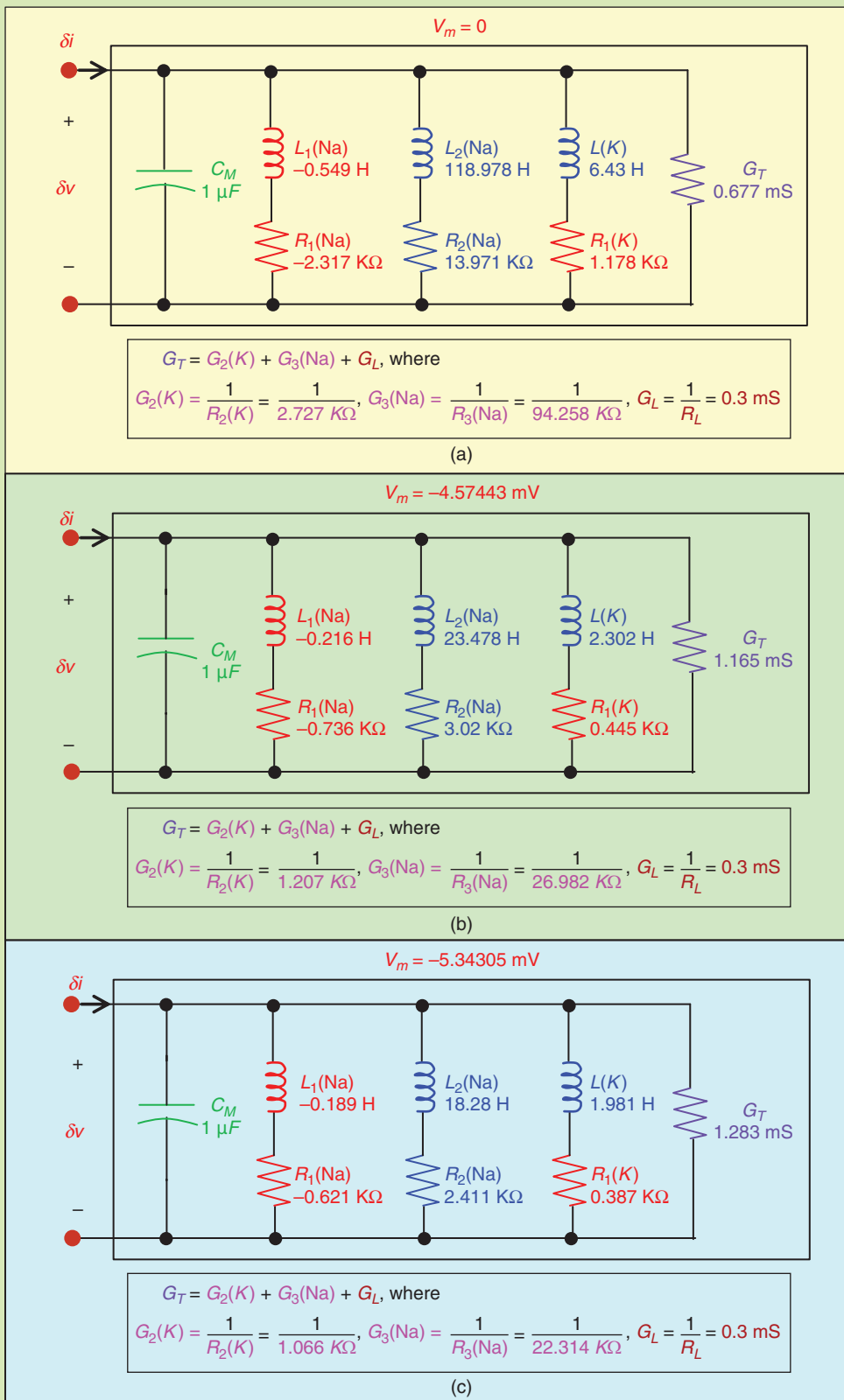


**Figure 20.** Small-signal memristive Hodgkin-Huxley axon circuit model at (a)  $V_m = 0$ ,  $V_K = -12 \text{ mV}$ , and  $V_{\text{Na}} = 115 \text{ mV}$ , (b)  $V_m = -4.57443 \text{ mV}$ ,  $V_K = -16.57443 \text{ mV}$ , and  $V_{\text{Na}} = 110.42557 \text{ mV}$ , (c)  $V_m = -5.34305 \text{ mV}$ ,  $V_K = -17.34305$ , and  $V_{\text{Na}} = 109.65695 \text{ mV}$ , respectively.

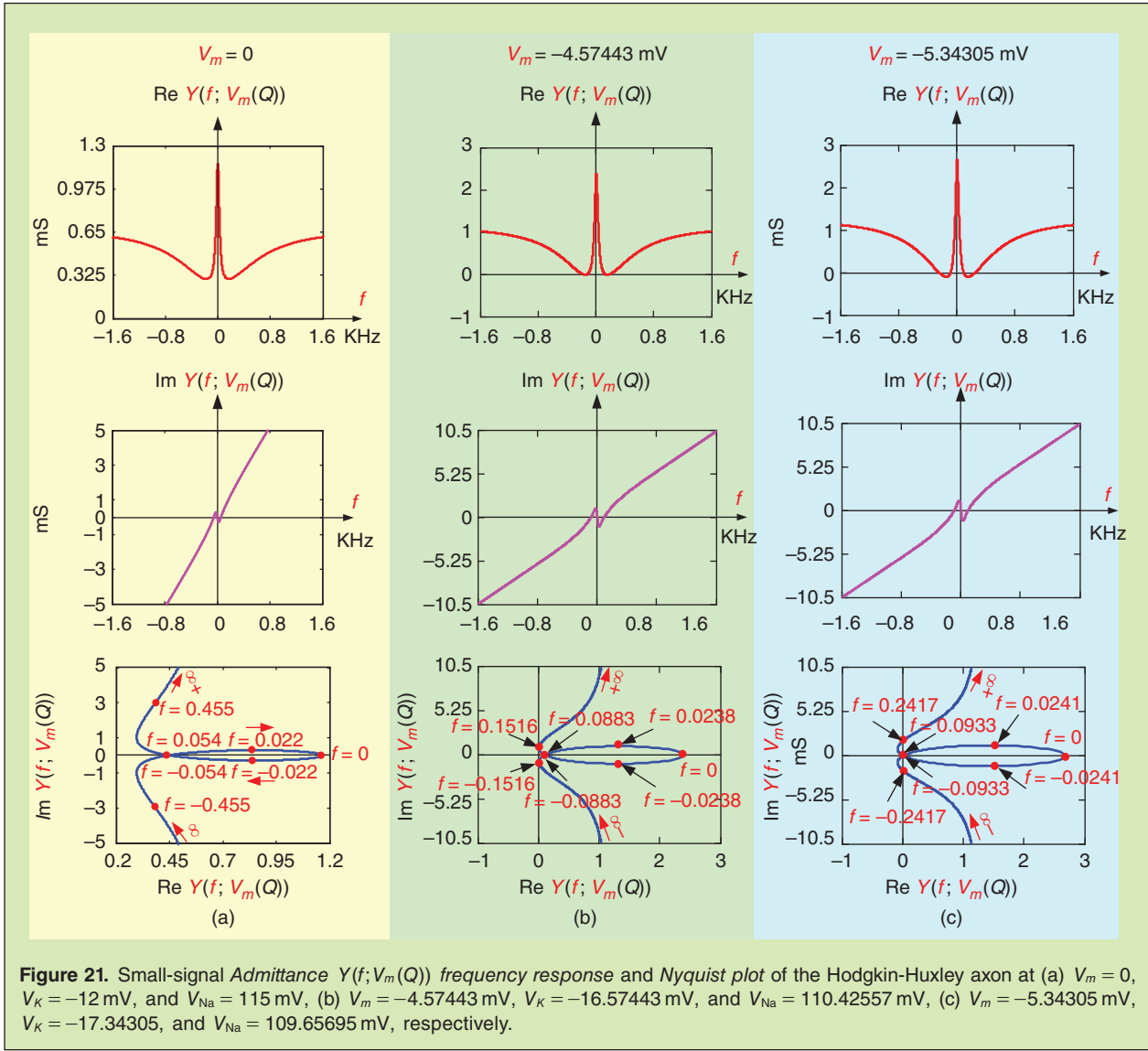


**Figure 21.** Small-signal Admittance  $Y(f; V_m(Q))$  frequency response and Nyquist plot of the Hodgkin-Huxley axon at (a)  $V_m = 0$ ,  $V_K = -12$  mV, and  $V_{Na} = 115$  mV, (b)  $V_m = -4.57443$  mV,  $V_K = -16.57443$  mV, and  $V_{Na} = 110.42557$  mV, (c)  $V_m = -5.34305$  mV,  $V_K = -17.34305$ , and  $V_{Na} = 109.65695$  mV, respectively.

The parameters of the small-signal equivalent circuit and coefficient of the sodium ion-channel memristor defined in (12) and (13) depend on  $v_{Na} = V_{Na}(Q_{Na})$  at the equilibrium point  $Q_{Na}$ . Figs. 17(a)–(d) show the variation of the inductances  $L_1(Na)$ ,  $L_2(Na)$ , resistances  $R_1(Na)$ ,  $R_2(Na)$ ,  $R_3(Na)$ , coefficients  $a_0, a_1, a_2$  and coefficients  $b_0, b_1, b_2$  of the small-signal sodium-ion channel memristor as a function of the sodium ion-channel memristor DC equilibrium voltage  $V_{Na}$ , respectively.

Fig. 18 shows the small-signal equivalent circuit, small-signal admittance frequency response,  $\text{Re } Y_{Na}(f; V_{Na})$  vs.  $f$ ,  $\text{Im } Y_{Na}(f; V_{Na})$  vs.  $f$ , and the Nyquist plot,  $\text{Im } Y_{Na}(f; V_{Na})$  vs.  $\text{Re } Y_{Na}(f; V_{Na})$  of the sodium ion-channel memristor at (a)  $V_{Na} = 115$  mV, (b)  $V_{Na} = 110.42557$  mV and (c)  $V_{Na} = 109.65695$  mV. These three voltages are chosen correspond to the three DC equilibrium voltages  $V_m = 0$ ,

$V_m = -4.57443$  mV, and  $V_m = -5.34305$  mV of the DC memristive Hodgkin-Huxley axon circuit model.

### C. Small-Signal Equivalent Circuit and Nyquist Plot of the Hodgkin-Huxley Axon Circuit Model

The small-signal Hodgkin-Huxley equivalent circuit about an external DC voltage  $V$  is shown in Fig. 19, where the potassium memristor and potassium Battery  $E_K$  in Fig. 13(a) are replaced by the small-signal equivalent circuit of the potassium memristor about its DC equilibrium point  $V_K = V - E_K$ . Similarly, the sodium memristor and sodium battery  $E_{Na}$  in Fig. 13(a) are replaced by the small-signal equivalent circuit of the sodium memristor about its DC equilibrium point  $V_{Na} = V + E_{Na}$ .

The admittance  $Y(s; V_m(Q))$  at the equilibrium point  $Q$  at  $V = V_m(Q)$  of the memristive Hodgkin-Huxley axon circuit model in Fig. 19 is given by [5]

$$Y(s; V_m(Q)) = G_T + \frac{1}{sL(K) + R_1(K)} + \frac{1}{sL_1(\text{Na}) + R_1(\text{Na})} \\ + \frac{1}{sL_2(\text{Na}) + R_2(\text{Na})} + sC_M,$$

where  $G_T = G_2(K) + G_3(\text{Na}) + G_L$ ,  $G_2(K) = 1/R_2(K)$ ,  $G_3(\text{Na}) = 1/R_3(\text{Na})$ , and  $G_L = 1/R_L$ . The circuit elements  $L(K)$ ,  $R_1(K)$  and  $R_2(K)$  from the small-signal equivalent circuit of the potassium memristor and the circuit element values  $L_1(\text{Na})$ ,  $L_2(\text{Na})$ ,  $R_1(\text{Na})$ ,  $R_2(\text{Na})$  and  $R_3(\text{Na})$  from the small-signal equivalent circuit of the sodium memristor are calculated from explicit formulas given in Table 3 and Table 4, respectively.

We can recast (15) into the form of a *rational function*

$$Y(s; V_m) = \frac{b_4s^4 + b_3s^3 + b_2s^2 + b_1s + b_0}{a_3s^3 + a_2s^2 + a_1s + a_0}, \quad (16)$$

where the 9 coefficients ( $a_0, a_1, a_2, a_3, b_0, b_1, b_2, b_3, b_4$ ) depend on the circuit elements in the small-signal circuit model in Fig. 19. The explicit formula defining each coefficient is reproduced in Table 5 from [5].

Substituting  $s = i\omega$  in (16), we obtain the following *small-signal Admittance* of the Hodgkin-Huxley axon circuit model at the DC equilibrium membrane voltage  $V = V_m(Q)$ :

$$Y(i\omega; V_m) = \frac{b_4(i\omega)^4 + b_3(i\omega)^3 + b_2(i\omega)^2 + b_1(i\omega) + b_0}{a_3(i\omega)^3 + a_2(i\omega)^2 + a_1(i\omega) + a_0} \\ = \frac{(b_0 - b_2\omega^2 + b_4\omega^4) - i(b_1 - b_3\omega^2)\omega}{(a_0 - a_2\omega^2) + i(a_1 - a_3\omega^2)\omega}. \quad (17a)$$

Separating Eq. (17) into its real and imaginary parts, we obtain (17b) and (17c), as shown at the bottom of the page.

The above equations are defined in terms of  $s = i\omega$ . If we substitute  $\omega = 2\pi f$ , then the above equations can be obtained as a function of frequency  $f$ . All graphs in this paper are plotted as a function of frequency  $f$ .

The small-signal memristive Hodgkin-Huxley axon circuit model in Fig. 19 is composed of a Capacitor  $C_M$ ,

three inductances  $L_1(\text{Na})$   $L_2(\text{Na})$ ,  $L(K)$ , three resistances  $R_1(\text{Na})$   $R_2(\text{Na})$ ,  $R_3(\text{Na})$ , two resistances  $R_1(K)$ ,  $R_2(K)$ , and a conductance ( $G_L$ ). The circuit elements and coefficients parameters depend on the DC axon membrane voltage  $V_m = V_m(Q)$  at the equilibrium point  $Q$ . Figs. 20(a)–(c) show the value of the circuit elements at equilibrium point  $V_m = 0$ ,  $V_m = -5.34305$  mV and  $V_m = -4.57443$  mV, respectively. The corresponding admittance  $Y(f; V_m(Q)) = \text{Re } Y(f; V_m(Q)) + i \text{Im } Y(f; V_m(Q))$  frequency response and Nyquist plot of the small-signal circuit model of the memristive Hodgkin-Huxley axon circuit model are shown in Figs. 21(a)–(c), respectively.

The first column in Fig. 21 at the DC equilibrium voltage  $V_m = 0$  corresponds to the DC steady state voltage measured across the Hodgkin-Huxley squid axon circuit model in Fig. 13(a), when  $I = 0$ . Hence, when there is no external stimulation signal ( $I = 0$ ), the squid axon has a *normalized* axon membrane voltage  $V_m = 0$ . When a small signal current source  $I = I_{\text{ext}} < 0$  is applied across the Hodgkin-Huxley circuit model<sup>3</sup>, Fig. 13(a), which corresponds to an external excitation signal, the DC memristive Hodgkin-Huxley axon circuit model in Fig. 13(b) is calculated to be a negative voltage  $V_m < 0$ . In particular, when  $I_{\text{ext}} = -7.8293 \mu\text{A}$ , our calculation gives a corresponding DC squid axon membrane voltage  $V_m = -4.57443$  mV. This corresponds to column 2 in Fig. 21 [5], [6]. At  $I_{\text{ext}} = -9.77004 \mu\text{A}$ , our calculation gives  $V_m = -5.34305$  mV. This corresponds to column 3 of Fig. 21 [5], [6].

Observe that  $\text{Re } Y(f; V_m(Q)) = 0$  at  $V_m = -4.57443$  mV in Fig. 21(b). Moreover, our calculation shows  $\text{Re } Y(f; V_m(Q)) < 0$  when  $V_m = -(4.57443 + \Delta V_m)$  mV for small positive increments in  $V_m$ . It follows from the *local activity principle* that the Hodgkin Huxley axon circuit model is at the *onset of the edge of chaos* at  $V_m = -4.57443$  mV, a *fundamental deep* result investigated extensively in [6].

<sup>3</sup>This external excitation signal summarizes the external stimulations from neighboring neurons via the neuron's dendrites.

$$\text{Re } Y(i\omega; V_m) = \frac{(a_0 - a_2\omega^2)(b_0 - b_2\omega^2 + b_4\omega^4) + (a_1 - a_3\omega^2)(b_1 - b_3\omega^2)\omega^2}{(a_0 - a_2\omega^2)^2 + (a_1 - a_3\omega^2)^2\omega^2} \\ = \frac{(a_3b_3 - a_2b_4)\omega^6 + (a_0b_4 - a_1b_3 + a_2b_2 - a_3b_1)\omega^4 + (a_1b_1 - a_0b_2 - a_2b_0)\omega^2 + a_0b_0}{a_3^2\omega^6 + (a_2^2 - 2a_1a_3)\omega^4 + (a_1^2 - 2a_0a_2)\omega^2 + a_0^2} \quad (17b)$$

$$\text{Im } Y(i\omega; V_m) = -\frac{[(a_1 - a_3\omega^2)(b_0 - b_2\omega^2 + b_4\omega^4) - (a_0 - a_2\omega^2)(b_1 - b_3\omega^2)]\omega}{(a_0 - a_2\omega^2)^2 + (a_1 - a_3\omega^2)^2\omega^2} \\ = \frac{a_3b_4\omega^7 - (a_1b_4 - a_2b_3 + a_3b_2)\omega^5 - (a_0b_3 - a_1b_2 + a_2b_1 - a_3b_0)\omega^3 + (a_0b_1 - a_1b_0)\omega}{a_3^2\omega^6 + (a_2^2 - 2a_1a_3)\omega^4 + (a_1^2 - 2a_0a_2)\omega^2 + a_0^2} \quad (17c)$$

Observe also that  $\operatorname{Re} Y(f; V_m(Q)) = 0$  and  $\operatorname{Im} Y(f; V_m(Q)) = 0$  at  $V_m = -5.34305 \text{ mV}$  in Fig. 21(c). This implies that the *admittance* function  $Y(s; V_m(Q))$  of the Hodgkin-Huxley axon circuit model has a zero  $s = 0$  (or equivalently, the impedance function  $Z(s; V_m(Q))$  has a pole at  $s = 0$ ) at  $V_m = -5.34305 \text{ mV}$ . This corresponds to the right boundary of the *edge of chaos* domain, and the onset of a *sub-critical Hopf Bifurcation*, which is the mechanism which gives birth to the *action potential* in the giant squid axon [6].

## V. Conclusion

Since *synapse* and *axons* are the two fundamental components of neurons responsible for computation and information processing in the brain, and since both synapses and axons can be emulated electronically by *locally-passive* memristors, and *locally-active* memristors [12], respectively, it follows that, from an information processing, memory, and learning perspective, *brains are made of memristors*. Moreover, since memristors are nano electronic devices, the aspect ratio between the “*footprints*” of an electronic neuron and an electronic synapse is more than three orders of magnitude, which is compatible with the corresponding aspect ratio between a biological neuron, and a biological synapse, it follows that memristors are the *right stuff* for building *brain-like machines*. The race is now on for the commercialization of low-power intelligent memristor-based brain-like computers that can outperform digital supercomputers on such routine tasks as facial recognition and associative memories that our brain excels.

## Acknowledgment

This work was supported in part by the US Air Force Grant FA9550-13-1-0136 and two National Research Foundation of Korea (NRF) grants funded by the Korea government (No. 2013R1A1A2062282 and 2013R1A2A2A01068683).



**Maheshwar Pd. Sah** received the B.E. in Electronics and Communication Engineering from Pokhara University, Nepal in 2005, M.E. and Ph.D. in Electronics Engineering from Chonbuk National University, Republic of Korea in 2010 and 2013 respectively. He is currently working as a Postdoctoral scholar in Chonbuk National University, Republic of Korea. His main research interests include Circuit design, Cellular Neural Network, Analog viterbi decoder, analysis of Memristor and Memristive System.

**Hyongsuk Kim** received the Ph.D. degree in Electrical Engineering from the University of Missouri, Columbia, in 1992. Since 1993, he has been a Professor with the Division of Electronics Engineering, Chonbuk National



University, Republic of Korea. From 2000 to 2002 and again from 2009 to 2010, he was with the Nonlinear Electronics Laboratory, EECS Department, University of California, Berkeley, as a Visiting Scholar. His current research interests include memristors and its application to Cellular Neural/Nonlinear Networks.



**Leon O. Chua** (Fellow, IEEE) received the M.S. degree from the Massachusetts Institute of Technology, Cambridge, in 1961 and the Ph.D. degree from the University of Illinois at Champaign-Urbana in electrical engineering, in 1964. He has been a Professor at the University of California Berkeley since 1971. In 2011, he was appointed a Distinguished Professor at the Technical University of Munich. He was awarded seven patents and 14 honorary doctorates. When not immersed in science, he relaxes by searching for Wagner’s leitmotifs, musing over Kandinsky’s chaos, and contemplating Wittgenstein’s inner thoughts. Prof. Chua received many awards including the first recipient of the Gustav Kirchhoff award, the Guggenheim Fellow award, and the European EC Marie Curie Fellow award. He was elected a foreign member of the Academia Europaea and of the Hungarian Academy of the Sciences. He was elected Confrerie des Chevaliers du Tastevin in 2000.

## References

- [1] E. R. Kandel, J. H. Schwartz, and T. M. Jessell, *Principles of Neural Science*, 4th ed. New York: McGraw-Hill, 2000.
- [2] L. Chua. “Memristor, Hodgkin-Huxley, and edge of chaos,” *Nanotechnology*, to be published.
- [3] S. H. Jo, T. Chang, I. Ebong, B. B. Bhadviya, P. Mazumder, and W. Lu, “Nanoscale memristor device as synapse in neuromorphic systems,” *Nano Lett.* vol. 10, no. 4, pp. 1297–1301, Mar. 2010.
- [4] A. L. Hodgkin and A. F. Huxley, “A quantitative description of membrane current and its application to conduction and excitation in nerve,” *J. Physiol.*, vol. 117, no. 4, pp. 500–544, Aug. 1952.
- [5] L. O. Chua, V. I. Sbitnev, and H. Kim, “Hodgkin-Huxley axon is made of memristors,” *Int. J. Bifurcation Chaos*, vol. 22, no. 3, pp. 1230011(1)–1230011(48), Mar. 2012.
- [6] L. O. Chua, V. I. Sbitnev, and H. Kim, “Neurons are poised near the edge of chaos,” *Int. J. Bifurcation Chaos*, vol. 22, no. 4, pp. 1250098 (1)–1250098(49), Apr. 2012.
- [7] L. O. Chua and S. M. Kang, “Memristive devices and systems,” *Proc. IEEE*, vol. 64, no. 2, pp. 209–223, 1976.
- [8] L. O. Chua, “Nonlinear circuit foundations for nanodevices, Part I: The four element torus” *Proc. IEEE*, vol. 91, no. 11, pp. 1830–1859, Nov. 2003.
- [9] R. G. Bartle, *The Elements of Real Analysis*, 2nd ed. New York: Wiley 1976.
- [10] L. O. Chua, *CNN: A Paradigm for Complexity*. Singapore: World Scientific, 1998.
- [11] K. S. Cole, *Membranes, Ions and Impulses*. Berkeley: Univ. California Press, 1972.
- [12] K. Mainzer and L. Chua, *Local Activity Principle*. Imperial College Press, Feb. 2013.